國立臺灣大學生命科學學院生化科學研究所

碩士論文

Institute of Biochemical Sciences

College of Life Science

National Taiwan University

Master Thesis

CRISPR-Cas9 技術於粒線體基因編輯之應用與對細胞功能之影響

Opportunities and Challenges in Repurposing CRISPR-Cas9 System for Mitochondrial Genome Editing

朱銘

Max Chu

指導教授：凌嘉鴻 博士

Advisor: Steven Lin, Ph.D.

中華民國一〇九年六月

June 2020

國立臺灣大學碩士學位論文
口試委員會審定書

CRISPR-Cas9 技術於粒線體基因編輯之應用與對細胞功能之影響
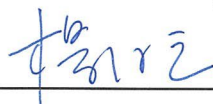## Opportunities and Challenges in Repurposing CRISPR-Cas9 System for Mitochondrial Genome Editing

本論文係朱銘君（R07B46012）在國立臺灣大學生化科學研究所完成之碩士學位論文，於民國 109 年 6 月 22 日承下列考試委員審查通過及口試及格，特此證明

口試委員：

_____（簽名）
（指導教授）

系主任、所長 _____（簽名）

（是否須簽章依各院系所規定）

i

謝辭

　　我所憧憬的研究是能在探究真理之時，與之產生連結進而創建生命中有價值的革新。這樣的理想必然須透過時間的累積與無數心力的付出方得實行。我很慶幸自己能藉由在生化科學研究所的碩士班期間投入基因編輯之研究，從而積累成此篇論文，並真切體會從事研究的所成所感。研究之路的顛簸總會不期而遇，其鍛鍊的是對結果之判斷與演繹，以調整實驗策略及方向。不論經過驗證後的種種假說是否成立，總能從中獲取經驗做作為後續研究的依據。另外，與前人的經驗交流亦為進展研究的有效參考。本篇研究即是依循此過程而成，亦憑藉了身邊許多人們的扶持與幫助，對此我誠心感謝。很謝謝楊維元老師及陳光超老師擔任我的口試委員，為此篇論文提供專業的見解與建議。謝謝凌嘉鴻老師在研究上的指導與協助，以及在處事上總是願意給予良好建議與支持，在此做研究獲得的學習與成長實屬可貴。同時也要謝謝馮聖富學長、洪欣如學姊、廖婉君學姊、王承宥在本研究上給予的種種協助，謝謝張耀仁學長、陳慧瑜學姊、黃日昇學長、俞安學姊、張正諭及凌嘉鴻老師實驗室歷來同仁們的互相幫忙。感謝爸爸、媽媽、哥哥對於我在生活上的莫大支持與鼓勵，也謝謝女友與朋友們生活上的陪伴。真心感謝以上人們參與了我在這段研究期間的生活與成長，也謝謝這段研究經歷帶給我的啟發和轉變。

本研究榮獲財團法人罕見疾病基金會

「第21屆罕見疾病博碩士論文獎助學金」獎助

謹於此特別致謝

中文摘要

　　粒線體對於細胞進行能量代謝及維持動態恆定而言至關重要，當粒線體基因突變可能導致粒線體功能缺失，甚至引發嚴重疾病。粒線體基因病變與修復機制的研究具有高度挑戰性，而其仰賴於粒線體基因編輯工具的開發。過去有研究團隊嘗試利用限制酶、人工合成之DNA內切酶 (如：ZFN或TALENs)剔除突變之粒線體基因。近年來由於CRISPR-Cas9技術在目標基因位點設計及基因編輯之方便性等優勢下興起，此技術亦有開發於粒線體基因編輯之潛力，然而目前已知對於輸送嚮導RNA (guide RNA)至粒線體之細胞機制的研究並不深入。在這篇研究中，我們對Cas9蛋白以及嚮導RNA分別修飾粒線體標的序列(mitochondria targeting sequence; MTS)，促使其有效率的進入粒線體中。我們在高解析度共軛焦顯微鏡下證實mito-Cas9能進入粒線體內。藉由反轉錄PCR分析，我們在粒線體萃取中發現有增量之mito-sgRNA。然而在開發應用於粒線體基因編輯之Cas9系統(mito-Cas9 system)時，我們發現在HeLa細胞中表現mito-Cas9會造成細胞毒性而導致細胞凋亡，其中存活的細胞則有關閉mito-Cas9表現之現象，且輸送mito-sgRNA至細胞中會造成粒線體基因數量減少。為了建立一套完善的基因編輯系統，我們致力對mito-Cas9的表達時間與強度進行優化以降低其造成的粒線體壓力。這套mito-Cas9系統的開發可望應用於粒線體之基因體研究以及粒線體基因病變之治療。

關鍵字

粒線體疾病、基因編輯、CRISPR-Cas9、粒線體RNA、基因治療

Abstract
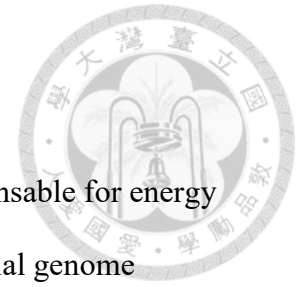
Mitochondria are essential organelles in eukaryotic cells, indispensable for energy production, metabolisms and homeostasis. Mutations in mitochondrial genome (mtDNA) are highly disruptive to mitochondrial functions and cause devastating diseases. The research of mtDNA repair and mutation pathogenicity is challenging, and the lack of good genetic tools is one of the main reasons. Genetic editing of mtDNA is not a new idea and has been demonstrated by using restriction enzymes and programmable nucleases such as Zinc-finger nucleases, Transcription activator-like effector nucleases and more recently CRISPR-Cas9. Each technique has its strengths and limitations, and this work focuses on CRISPR-Cas9 system for mtDNA editing. RNA-guided DNA cleavage of Cas9 allows fast reprogramming of Cas9 target specificity. However, mitochondrial localization of the guide RNA requires specialized RNA import mechanisms that remain poorly understood. Here we describe the modifications of Cas9 protein (mito-Cas9) and guide RNA (mito-sgRNA) to achieve robust and specific mitochondrial localization. We present high-resolution confocal microscopic images of mitochondrial localization of mito-Cas9, which carries a novel mitochondrial targeting sequence. We also detected enrichment of mito-sgRNA, which carries a unique RNA hairpin, in the purified mitochondrial extract by reverse transcription-PCR using endogenous 5S rRNA as a benchmark. However, the reconstitution of mtDNA-targeting Cas9: guide RNA ribonucleoprotein complexes is difficult, owing to high cellular toxicity of mito-Cas9. The expression of mito-Cas9 alone in HeLa cell line by plasmid transfection induced mitochondrial fragmentation and cell death within two days. The surviving cells had completely silenced the expression of mito-Cas9 after three weeks. The transfection of *in vitro* transcribed mito-sgRNA caused reduced copies of mtDNA in HeLa cell line within one day. Strategies

are needed to fine tune the expression level and timing of the mito-Cas9 system to avoid

undesirable mitochondrial stress and enable unbiased detection of mtDNA cleavage.

Successful establishment of a robust CRISPR-based mtDNA editing system will help

advance mtDNA research and offer strategies for therapeutic correction of pathogenic

mtDNA mutations.

Key words

Mitochondrial genome editing, CRISPR-Cas9, mitochondria-targeting Cas9,

mitochondria RNA import, mito-Cas9 system

Table of Contents

Table of Figures

Table of Tables

Introduction

1. Significance of mitochondria

Mitochondria is an essential organelle in eukaryotes for producing adenosine triphosphate, regulation of metabolism, and cell death[1]. Mitochondria have their own genome (mtDNA). The human mtDNA is a 16569 base-pair, intron-less circular double-strand DNA. It encodes 37 essential genes which include 13 protein subunits, 22 tRNAs, and two rRNAs[2]. Because of the fundamental biological roles and concise genetic organization in mitochondria, it is important to maintain the mitochondria genome integrity for cellular homeostasis. However, mtDNA are often exposed to oxidative stress caused by free radicals generated via oxidative phosphorylation that can lead to mtDNA mutations. The accumulation of mtDNA mutations can predispose individuals to neurodegenerative and myopathy disorders, such as Leber Hereditary Optic Neuropathy (LHON), Leigh syndrome, Kearns-Sayre syndrome (KSS), and Myoclonic Epilepsy with Ragged Red Fibers syndrome (MERRF)[3-7]. To address these disease-related mtDNA mutations, the development of mitochondria genome editing tools can bring great potential for therapeutic corrections.

2. Gene editing strategies for mtDNA manipulation

Mutations on mtDNA may lead to dreadful disorders, yet it is not completely intolerable. In average, a human cell can contain 1000 copies of mtDNA. Among those copies, there may be wild type and mutant mtDNA all at once. This phenomenon is called mtDNA heteroplasmy. The mitochondrial functions are disrupted if the mutant mtDNA proportion exceeded the threshold. Although the threshold level varies in different tissues, common mitochondrial defects hold a threshold value in the range of 60%-90%[8]. Because of the lack of efficient DSB repair in mitochondria, a more feasible

strategy is to eliminate the mutant mtDNA by inducing DNA degradation. It is reported that mtDNA linearization would lead to heteroplasmic shift (mutant mtDNA reduction and wild type mtDNA repopulation)[9,10]. Also, damaged mtDNA could induce mitophagy in cells to clear out the malfunctioning mitochondria[11].

To target the mutant mtDNA, gene-editing techniques have been developed to meet the needs. Those include mitochondria-targeting restriction enzymes, zinc finger nucleases (ZFN), and transcription activator-like effector nucleases (TALENs). Mitochondria-targeting restriction enzymes have proven to trigger heteroplasmic shift without off-target effect in mouse model and human culture cell lines[9,12-14]. However, the limitation is that only two out of nearly 200 pathogenic mutation sites in mitochondria can be targeted by these restriction enzymes.

The limitation of restriction enzymes made ZFN and TALENs stand out for targeting a broader range of mutant mtDNA. These two gene-editing technologies are programmable. Mitochondria-targeting ZFNs (mito-ZFN) have been reported to target a 12-nucleotide sequence on mutant mtDNA, and specifically remove the mutant which is only one-nucleotide different from the wild type mtDNA[15]. Also, mito-ZFN has demonstrated mtDNA reduction with a heteroplasmic shift towards the wild type mtDNA by targeting m.8993T>G mutation in human cells. Mitochondria-targeting TALENs (mito-TALEN) can reduce human mutant mtDNA in mammalian oocytes[12,16]. Mito-TALENs can also permanently eliminate mtDNA with single nucleotide variation or deletion in patient-derived cells[17,18].

Mito-ZFN and mito-TALENs have provided progress in mtDNA targeting. However, it is still necessary to introduce more efficient genetic tools for mtDNA targeting. Therefore, there is a need to develop the flexible CRISPR-Cas9 gene-editing technology for mtDNA manipulation.

3. CRISPR-Cas9 gene-editing technology

The CRISPR-Cas nucleases are capable of specifically recognizing a target sequence with the guidance of a CRISPR RNA (crRNA), and induce cleavage of the target nucleic acid. The CRISPR-Cas9 system has become the prominent gene-editing technology since its establishment in 2012[19]. With a GAAA tetraloop linking the crRNA and trans-activating crRNA (tracrRNA) to form a single guide RNA (sgRNA) molecule, the CRISPR-Cas9 system simply requires two components for DNA targeting, the Cas9 protein and the sgRNA molecule. CRISPR-Cas9 system enables sequence-specific gene editing for nearly any target DNA by changing the sgRNA sequence. However, the applications of CRISPR-Cas9 are mainly focused on nuclear genome editing. Mitochondrial genome editing with CRISPR-Cas9 technology has not been fully developed.
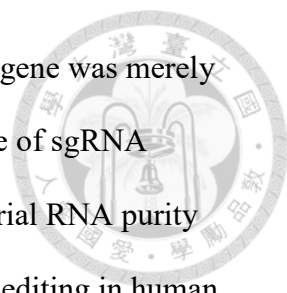
Adapting CRISPR-Cas9 technology to mtDNA editing remains challenging because of the lack of efficient techniques to transport the complete Cas9 system, the Cas9 protein, sgRNA, and DNA template, into the mitochondria. For the Cas9 protein import, it is critical to find a suitable MTS to guide Cas9 into the mitochondrial matrix through the pre-sequence pathway. As for sgRNA import, a RNA MTS is required to facilitate the translocation of sgRNA into the mitochondria. However, there are limited RNA MTSs found for mitochondrial import. Also, these RNA MTSs rely on PNPase recognition, a still unclear mechanism, to localize within the mitochondria. Precise DNA editing requires a DNA template to allow DNA repair of the cleavage site through HDR. While DSB repair were found in mitochondria, there was lacking evidence of HDR events[20-22]. Also, DNA import mechanisms are not fully understood[23]. Hence, it is more reliable to manipulate the mtDNA by mutant mtDNA elimination followed by

mtDNA replication. Even with the establishment of a mito-Cas9 system that can efficiently translocate into the mitochondria, it is still essential to exclude mitochondria stress accumulations caused by the mito-Cas9 system that interferes with the mitochondria function.
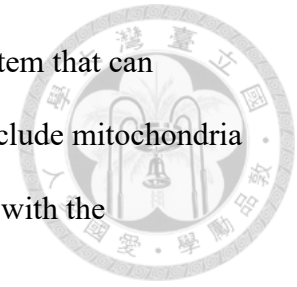
4. CRISPR-Cas9-based mtDNA editing

There are currently five published research articles focusing on mitochondria-targeting CRISPR-Cas9 (mito-Cas9)[24-28]. Jo *et al.* first reported mtDNA editing with mito-Cas9 in 2015[24]. They claimed to discover that non-MTS-modified FLAG-Cas9 could localize to mitochondria for mtDNA editing. They demonstrated mtDNA editing in HEK293T cells with FLAG-Cas9 and sgRNA targeting Cox1 and Cox3, which led to reduction of mtDNA copy number detected by qPCR and disruption of mitochondrial protein homeostasis. Although they also performed mtDNA cleavage by mito-Cas9 that caused mitochondrial membrane potential disruption and cell growth inhibition, their work caused a discussion on whether Cas9 with nuclear-localization signal (NLS) and non-modified sgRNA could localize in the mitochondria[29]. Loutre *et al.* demonstrated mtDNA editing in a human culture cell line (HepG2)[25]. They have provided evidence of the mitochondria import of mito-Cas9 and mito-sgRNAs. However, their mito-Cas9 system requires a pair of mito-sgRNAs, one targeting on the non-coding region and the other targeting Cyt-b, to induce mtDNA depletion detected by qPCR analysis. Bian *et al.* has published their work on mtDNA editing in human cell line (mitochondrial DNA target sites: *ND1* and *ND4*) and zebrafish embryo (mitochondrial DNA target sites: *dloop-1* and *dloop-2*)[26]. They showed that their mito-Cas9 can induce mtDNA reduction detected by qPCR. They also performed gene knock-in with an exogenous single strand DNA and validated the results by PCR and Sanger sequencing. However, their gene

4
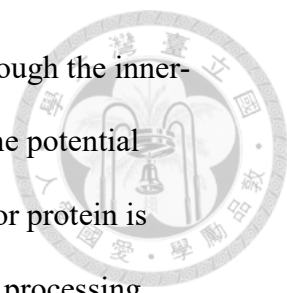
knock-in detection by PCR could not exclude the possibility that the gene was merely knocked-in to the pseudogenes within the nucleus. Also, the evidence of sgRNA localization in mitochondria was not solid as the detail of mitochondrial RNA purity was not provided in their work. Hussain *et al.* demonstrated mtDNA editing in human cell line (HEK293K) and primary mouse embryonic fibroblast with their mito-Cas9 and RP-loop gRNA targeting *ND4*, causing reduction of mtDNA and ND4 transcripts detected by qPCR and RT-qPCR, yet did not provide evidence for mitochondrial localization of Cas9[27]. To establish a robust mito-Cas9 system for mtDNA manipulation, efficient transport of Cas9 and sgRNA into the mitochondrial matrix is necessary.

5. Mitochondrial protein import mechanism

Cas9 protein needs modifications for mitochondrial import. In human cells, a majority of mitochondrial proteins (about 1500 genes) are encoded in the nuclear genome. While these genes are translated to precursor protein in the cytosol, they could go through mitochondria import machinery.

Since we aim to deliver Cas9 into the matrix for mtDNA targeting, we focused on the pre-sequence pathway for mitochondrial import into inner membrane and matrix. Translocase of the outer membrane (TOM) is the common entrance for precursor protein mitochondrial import. Most of the precursor proteins have MTS at the N-termini for TOM recognition. The MTS usually consists of 15-50 amino acids that could form positively charged amphipathic α-helix. The hydrophobic surface of MTS could be recognized by TOM20 and the positively charged surface is recognized by TOM22[30-32]. TOM20 and TOM22 assist the precursor protein to pass through the outer membrane. Then as translocase of inner-membrane 23 (TIM23) recognizes the protein in the

intermembrane space, TIM23 can allow precursor protein to pass through the inner-membrane (the energy comes from ATP hydrolysis and the membrane potential generated through the electron transfer chain)[32,33]. While the precursor protein is transported into the matrix, the MTS is cleaved by the mitochondrial processing peptidase (MPP), and the protein would fold into its mature form with the aid of mitochondrial chaperons[34]. Since the protein folding is accomplished after mitochondrial import, the strategy is to deliver Cas9 and sgRNA separately so that the folded Cas9 can form an RNP complex with sgRNA within the mitochondria matrix

6. Mitochondrial RNA import

Unlike mitochondrial protein import, the import pathways for RNA remains obscure. It is known that several nuclear-encoded ncRNAs conjectured to facilitate translation and mitochondrial DNA replication in mitochondria, such as 5S rRNA, RNase P RNA, and RNase MRP RNA, are imported into the mitochondria[35-37]. A putative mechanism is that multifunctional protein PNPase could be involved in the RNA translocation into mitochondria. PNPase, encoded by *PNPT1* gene in human, was at first recognized as an evolutionarily conserved 3' to 5' exonuclease from bacteria[38,39]. It is found to function as poly(A) polymerase in *E. coli* and plant chloroplast[40,41]. Human PNPase is a homotrimeric complex located mainly in the intermembrane space and partially in the matrix. It is postulated that PNPase can recognize the RNA secondary structure. Meanwhile, how the RNAs can pass through the outer membrane and how PNPase facilitate the RNA import into the matrix are still questions to be solved. Given these unknown questions, we modified the sgRNA with the secondary structure to verify the postulation.

7. Specific aims of this study

The ultimate goal of this study is to establish a robust mito-Cas9 system for mitochondrial genome editing. Previously, we identified a suitable MTS for mitochondrial import of Cas9. Also, RNA MTSs were found for transporting sgRNA into mitochondria. Based on these achievements, my further aims are: (1) optimization of mito-Cas9 expression in cells; (2) evaluation of the toxicity and cellular effects from mito-Cas9 and mito-sgRNA expression; (3) demonstration of mtDNA targeting by the mito-Cas9 system. The success of this work can build up CRISPR-Cas9 based mitochondrial genome editing technology that can be applied for mitochondrial genome research and therapeutic approaches for mitochondria genetic defects.
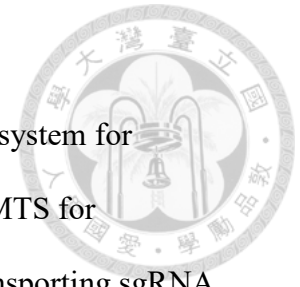
Results

1. A novel MTS for mito-Cas9 import into mitochondria

To deliver mito-Cas9 into mitochondria, we studied how nuclear-encoded mitochondrial proteins translocate into mitochondria biologically. It has been shown that those proteins enter the mitochondria through a co-translational process (Figure 2)[42]. When the peptide chain is synthesized by the ribosome, the mitochondria targeting sequence (MTS) will first be recognized by mitochondrial import receptors (TOM20, TOM22) on the mitochondrial outer membrane, and allow the peptide chain to enter mitochondria. After localizing at the correct intra-mitochondrial site, the mitochondrial protein can be folded into its mature form to perform its function. Based on this study, we searched for the MTSs on nuclear-encoded mitochondrial proteins, expecting them to be the ideal MTS for Cas9 translocation. We tested MTSs from cytochromes C oxidase subunit 8A (COX8A), cytochrome C oxidase subunit 4 (COX4P), acetyl-CoA carboxylase 2 (ACACB), glycine dehydrogenase (GLDC), DNA polymerase subunit gamma-1 (POLG), and monofunctional C1 tetrahydrofolate synthase(MTHFD1L) by fusing the putative MTS sequence to *cas9* gene in a series of plasmids and expressing these fusion proteins in HeLa cells through lipofectamine transfection. The MTS-Cas9 localization was analyzed by confocal microscopy and immunostaining against a FLAG fusion tag. We used MitoTracker Deep Red to stain the mitochondria to see whether the MTS-Cas9 could co-localize with mitochondria. Since the COX8A MTS and COX4P MTS were more well-studied MTSs for mitochondria import of small proteins, we expected that the mitochondria translocation of a large protein as Cas9 required MTSs from large mitochondrial proteins (over 100 kDa), such as ACACB, GLDC, POLG, and MTHFD1L MTS. The results showed that most of the MTSs failed to facilitate Cas9 import into the mitochondria, as the anti-FLAG signals were not overlapped with the

MitoTracker signals (Figure 3). Fortunately, we were able to find a MTS, the MTHFD1L MTS, that is suitable for Cas9 translocation into the mitochondria, as the anti-FLAG signals were highly overlapped with the MitoTracker signals, demonstrating the co-localization of mito-Cas9 and mitochondria (Figure 4, S. figure 1).

2. Mito-Cas9 expression leads to cellular abnormality

Although the construction of mito-Cas9 that can localize into the mitochondria is a promising result, it remains challenging to perform mtDNA targeting due to the low transfection efficiency, mito-Cas9 toxicity, and loss of mitochondria localization while over-expressed mito-Cas9 (Figure 5, S. figure 2). As we transfected the mito-Cas9 plasmid by Lipofectamine 3000 reagent into HeLa cells and evaluated the cell morphology via confocal microscopy. We found that the expression of mito-Cas9 after 1 day led to morphological changes that could cause cell death since most of the cells with mito-Cas9 expression showed aberrant morphology with plasma membrane vesicles and some even turned into cell debris (Figure 5, S. Figure 2D-F) As mito-Cas9 was over-expressed in the cells, the mitochondria started to turn vesicular instead of maintaining its reticular form, and the anti-FLAG signals could not co-localize with the MitoTracker signals, indicating that the localization of mito-Cas9 began to concentrate within the cytosol. However, the toxic effects including the change of cell morphology and mitochondria condition could also be found in Cas9 expression in the cells (S. Figure 2A-C). With confocal imaging data, it is difficult to determine whether the mitochondria localization of mito-Cas9 could cause additional stress to the cells compared to Cas9. Nevertheless, the results indicate that both Cas9 and mito-Cas9 over-expressions could be strong stressors to the cells, which make fine-tuning of the gene expression level a necessity to avoid excessive cell toxicity. Also, the current

9

transfection condition could only yield a portion of the cell population with mito-Cas9 expression (Figure 5), indicating the need for optimization of transfection efficiency.
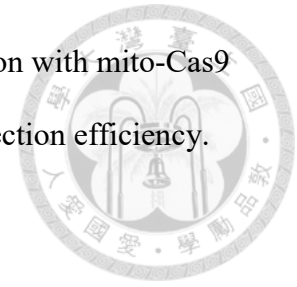
3. Mito-Cas9 transfection efficiency optimization

To overcome the low efficiency of mito-Cas9 transfection, we have set out to test the optimal transfection efficiency for mito-Cas9 expression. First, we performed lipofection and electroporation of a mito-Cas9-turbo GFP plasmid in HeLa cells on a 35-mm glass bottom dish and analyzed the cells by flow cytometry. The transfection efficiency was determined by analyzing the GFP signals and the dead cells were stained by Zombie violet dye to determine the cell viability. It turned out that electroporation caused a viability lower than 30% with merely 1% efficiency regardless of the plasmid dosage from 0.5 ug to eight ug (Figure 6A, B). As for lipofection, the transfection efficiency could be up to 12% with a viability around 70% for plasmid dosage two to four ug (Figure 6C, D). Moreover, we noticed that by transferring the performance of lipofection from 35-mm glass bottom dish to 24-well plate with the same condition, including the cell density, amount of lipofectamine reagent and plasmid DNA, the lipofection efficiency could be higher. This result indicated that compared to 35-mm glass bottom dish, performing transfection in 24-well plate was a more suitable approach for optimization, likely due to the flatness of the bottom surface so that the plasmid-lipofectamine complex could spread out better throughout the cells. Hence, we further optimized the transfection efficiency by testing different lipofectamine 3000 to plasmid ratio in the 24-well plate set up. The results showed that four ul lipofectamine to four ug condition had the highest efficiency (40%) among the condition tested (Figure 7B). Also, the trend showed it was likely that the lipofection efficiency could

10

still be optimized with higher amount of lipofectamine 3000 and plasmid than four ul
and four ug respectively.

4. Doxycycline-inducible mito-Cas9 stable cell line construction
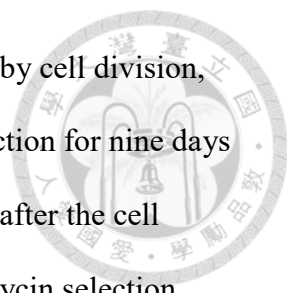
After finding an efficient mito-Cas9 for mitochondrial import, we also set out to
establish an inducible mito-Cas9 expression system in HeLa cell line via lentiviral
transduction as an alternative approach to overcome the low transfection efficiency
issue and establish stable mito-Cas9 expressing clones (Figure 8). We delivered a gene
cassette with mito-Cas9-GFP driven by tetracycline responsive element and puromycin
N-acetyltransferase (PAC), a puromycin resistance gene, to select the cells with the
gene cassette integrated into the genome by lentiviral transduction. The cells survived
from puromycin selection were sorted out by single cell sorting followed by cell
expansion for three weeks to synchronize the genomic condition within the cell
population. We expect that the resulting cell line could yield a nearly 100% of mito-
Cas9 expression among the cell population. However, as we performed puromycin
selection followed by mito-Cas9 induction and evaluated the expression rate by flow
cytometry, we found that the overall induction rate for each resulting cell line was less
than 10% (Figure 9). Since the PAC expression was confirmed and mito-Cas9 could be
expressed in partial cells, we assumed that the low expression rate was due to the
cellular response that selectively turned off the toxic mito-Cas9 expression. To
elaborate, there could be leaky expression of mito-Cas9 without doxycycline induction
after lentiviral transduction. As the mito-Cas9 was toxic to the cells, it might activate
cellular responses to genetically suppress mito-Cas9 expression, resulting an inefficient
inducible mito-Cas9 system with PAC expression remained to allow survival from the
puromycin selection.

11

5. mito-Cas9 cell line preparation via puromycin selection

Given that the mito-Cas9 expression might be selectively eliminated in cells due to its toxicity, we modified our expression system to reduce mito-Cas9 expression by replacing the CAG promoter with an hPGK promoter (Figure 10)[43]. Moreover, in order to assure the puromycin selection for mito-Cas9 positive cell line, we tethered the PAC gene to the mito-Cas9 driven by the same promoter. At first, we tried to deliver this mito-Cas9 expression system by lentiviral transduction yet the approach was unsuccessful as hardly any cells survived from puromycin selection. As the lentivirus packaging and transduction were previously successful in other constructs, we assumed the problem arose from the difficulty to express sufficient PAC to become resistant to puromycin as lentiviral transduction could yield low copy numbers and additionally it is expressed after mito-Cas9 that could result in a less efficient expression.

Since the plasmid construct originally designed for lentivirus packaging theoretically could also perform gene expression by transfecting the plasmids into the cells, we utilized lipofection to deliver this mito-Cas9 expression system into HeLa cells (Figure 11). After the puromycin selection, we successfully observed an enriched population of mito-Cas9 expression under confocal microscopy. By detecting the mito-Cas9 expression with anti-FLAG, most of the cells presented fluorescent signals, suggesting that this expression system was capable of establishing mito-Cas9 positive cell line (Figure 12). Theoretically, if the gene expression system could integrate into the genome through homologous recombination, there were chances to generate the mito-Cas9 expressing cell line. We continuously cultivate the cell line in puromycin condition. During continuous puromycin selection for 12 more days, we observed cell death that gradually reduced the cell population, which was expected since most of the

doi:10.6342/NTU202001420
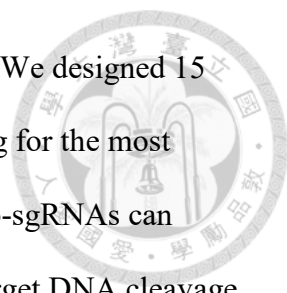
cells would lose their transient expression of PAC within two weeks by cell division, plasmid diffusion and degradation. Then, we paused puromycin selection for nine days to allow cell expansion and re-selected the cells by puromycin again after the cell expansion. We speculated that the cells survived from the last puromycin selection could be a cell line that was puromycin resistant and stably expressed mito-Cas9. However, as we analyzed the mito-Cas9 expression of those cells re-selected by puromycin, the mito-Cas9 expression was barely observed (Figure 13). We verified the low signal intensity was not the cause of the problems in immunofluorescence as the same reagents and protocol continuously worked on other samples. Since we further confirmed the existence of the exogenous gene in the mito-Cas9 negative yet puromycin resistant cell line by PCR (Figure 14) and Sanger sequencing, the explanation for the loss of mito-Cas9 expression could be the cellular response degrading the mito-Cas9 protein in a post-translational state.

6. Modified mito-sgRNAs maintain Cas9 cleavage activity

The mechanism for nuclear-encoded mitochondrial RNA to enter mitochondria is still debatable. One of the possible pathways is through polynucleotide phosphorylase (PNPase), a multifunctional protein localized in the inner-membrane space and partially in the matrix (Figure 15). PNPase is reported to be involved in the mitochondrial import of nuclear-encoded non-coding RNAs. After gene knock-out of *PNPT1* (PNPase-encoded gene), the mitochondrial import for those RNA transcripts is blocked[44]. This showed that PNPase could be one of the mediators for mitochondrial RNA import.

To import sgRNA into mitochondria, we linked the sgRNA with RNA motifs derived from 5S rRNA, RNase P RNA, RNase MRP RNA, and yeast tRNA[lys], that have been reported to be able to enter mitochondria (Figure 16). We hypothesized that these

RNA MTS-linked sgRNAs can enter mitochondria through PNPase. We designed 15 mito-sgRNAs for mitochondrial import (Figure 17). Before screening for the most efficient mito-sgRNA, it is essential to make sure whether these mito-sgRNAs can reconstitute to a ribonucleoprotein complex with Cas9 and induce target DNA cleavage. Therefore, we performed *in vitro* cleavage assay by combining Cas9 protein, *in vitro* transcribed mito-sgRNA, and target DNA substrate followed by 37°C incubation. After agarose gel electrophoresis to analyze the DNA cleavage efficiency, we noticed that RNA modifications on either 5' end only or both ends caused lower DNA cleavage efficiency as the band intensities of the cleavage products were lighter, compared to the cleavage efficiency of the sgRNA without modifications (S. figure 3). However, RNA modifications in the internal region did not affect DNA cleavage efficiency. The results suggested that the sgRNA modifications on 5' end might affect its folding, thereby influence the reconstitution of Cas9 RNP complex and target DNA cleavage activity.

7. PNPase and PNPase-mediated RNAs exist in HeLa mitochondria

Prior to analyzing the mitochondrial import efficiencies of mito-sgRNAs, we set out to demonstrate the gene expression of PNPase as well as PNPase-mediated nuclear-encoded RNAs in mitochondria. The establishment of these results can support our hypothesis for mitochondrial import of mito-sgRNAs. We used MitoTracker Deep Red to detect the mitochondria and anti-PNPase to detect PNPase. As the MitoTracker signals and anti-PNPase signals were highly overlapped within the cells. We confirmed that PNPase localizes at mitochondria in HeLa cell line (S. figure 4).

To evaluate the abundance of nuclear-encoded non-coding RNAs in mitochondria, we purified the mitochondrial RNA from HeLa cells and analyzed the RNA levels by RT-qPCR (S. figure 5 and 6). In our pipeline of mitochondrial RNA extraction, we

treated RNase A/T1 to eliminate the contamination of cytosolic RNAs with the purified

mitochondria to assure mitochondrial RNA purity for RT-qPCR analysis (S. figure 5B).

The results showed that we were able to detect and estimate the levels of nuclear-

encoded RNAs in mitochondria (S. figure 7).
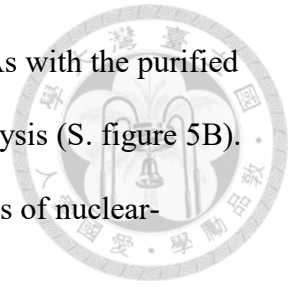
8. Modified mito-sgRNAs facilitate mitochondria translocation

Our mtDNA targeting approach relies on the delivery of mito-Cas9 expression

system and *in vitro* transcribed mito-sgRNA. We supposed this approach could lower

the possibility of off targeting on the pseudogenes in the nucleus since the mito-sgRNA

would be less able to remain in the nucleus compared to plasmid expression. Since we

have established a method to quantify target RNA levels in mitochondria, we could set

out to determine the mitochondrial translocation efficiency of our *in vitro* transcribed

mito-sgRNAs. First, we performed a time course assay to determine the timing of the

highest mito-sgRNA abundance within the cell after RNA transfection (S. figure 8A).

We used mito-sgRNA51 as the representative mito-sgRNA for transfection. After each

time period, three hours, six hours, nine hours, and 12 hours post-transfection, the total

RNA was extracted from the cells and the mito-sgRNA51 abundance was analyzed by

RT-qPCR. The results showed that the mito-sgRNA51 abundance relative to M16S

began to increase until the nine-hour time point, and dropped at the 12-hour time point

(S. figure 8B). After determining the optimal time point of mito-sgRNA abundance, we

transfected equal quantity of the mito-sgRNAs into HeLa cells to evaluate their

translocation efficiency by analyzing the mito-sgRNA abundance in mitochondria.

After 9-hour incubation, we extracted the mitochondrial RNA for RT-qPCR analysis.

We calculated the relative amount of mito-sgRNAs to 5S rRNA and found that mito-

sgRNA51 had the highest translocation efficiency among all the tested mito-sgRNAs (S. figure 9).

Although the relative mito-sgRNA translocation efficiencies were determined, we wanted to further understand the mito-sgRNA localization within the cells by confocal imaging. Previously in the lab, RNA detection methods by fluorescent dye labeling for mito-sgRNA visualization have been tried yet the results were unsuccessful with undesirably low signal intensity. Hence, we alternatively tested an *in situ* hybridization method that included an rolling circle amplification process that could amplify the signal intensity by fluorescent labeled detection probe[45]. We have been able to detect human β-actin with clear signals in HeLa cells by this method (Figure 18), which makes it a promising approach for mito-sgRNA detection.

9. Mito-sgRNA transfection efficiency optimization

After determining the highest mitochondrial translocation efficiency of mito-sgRNA51, we could use our mito-Cas9 coupled with mito-sgRNA51 as our mito-Cas9 system for mtDNA targeting assays. Since our mtDNA targeting approach is based on the delivery of *in vitro* transcribed mito-sgRNA, the transfection efficiency of mito-sgRNA was therefore important. We tested the transfection efficiency in HeLa cells by Lipofectamine 2000 reagent and RNAi MAX reagent for mito-sgRNA51. Nine hours after transfection, we extracted the total RNA and analyzed the mito-sgRNA abundance in the cells by RT-qPCR. The results showed that transfection with Lipofectamine 2000 could perform five-fold transfection efficiency compared to RNAi MAX (Figure 19). By performing RNA transfection with 0.6 ul Lipofectamine 2000 reagent, 14 pmol of mito-sgRNA51 could yield the highest transfection efficiency compared to seven pmol and 21 pmol condition. As for RNAi MAX transfection, the transfection efficiency was

16

slightly increased from seven pmol to 21 pmol. Among the condition tested, the highest mito-sgRNA51 transfection efficiency was using 0.6 ul Lipofectamine 2000 to 14 pmol mito-sgRNA51.
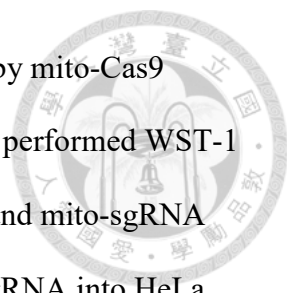
10. mtDNA targeting by mito-Cas9 system

Since we could use the puromycin selection strategy to enrich a cell population with mito-Cas9 expression, we set out to evaluate the mtDNA targeting efficiency of the mito-Cas9 system based on this expression strategy coupled with *in vitro* transcribed mito-sgRNA transfection (Figure 20). We delivered the mito-Cas9 plasmid into HeLa cells by lipofection and performed puromycin selection. Subsequently, we used Lipofectamine 2000 reagent to transfect the ND4 targeting mito-sgRNA into the cells. One day after mito-sgRNA delivery, the cellular DNA was extracted by the Quick-DNA™ Miniprep Plus kit. We analyzed the ND4 level relative to HBB, a nucleus encoded gene as internal control, by qPCR to determine the targeting efficiency. Since the mtDNA cleavage leads to DNA degradation[46,47], we also analyzed the M16S level relative to HBB to inspect the mtDNA condition resulting from mtDNA targeting. We found that the mito-Cas9 system could cause a reduced mtDNA level (Figure 21). However, this effect was also shown in mito-sgRNA (mito-sgRNA51 as well as mito-sgRNA36) transfection only. We speculated that the mtDNA interference of mito-sgRNA was the cause of gene interruption in the cells that led to mitochondrial malfunctioning.

11. Mitochondria physiology and cell viability influenced by mito-Cas9 system

As we noticed that the mito-Cas9 system, both mito-Cas9 and mito-sgRNA, could be toxic to the cells, we began to scrutinize the toxicity of the mito-Cas9 system. The

17

evaluation could help us understand more detailed influence caused by mito-Cas9 system and determine the feasibility of the expression strategies. We performed WST-1 assay to analyze the cell viability affected by mito-Cas9 expression and mito-sgRNA delivery (Figure 22). After the transfection of mito-Cas9 and mito-sgRNA into HeLa cells respectively, WST-1 reagent was added to the cell medium to allow the mitochondrial succinate-tetrazolium-reductase system within the cells to convert the WST-1 to formazan, which could be detected by ELISA reader at 440 nm absorbance. The higher converting rate of WST-1 reagent to formazan indicated the higher cell viability. The results showed that mito-Cas9 expression could cause a 30% decrease of cell viability in HeLa cell line, and the mito-sgRNA51 delivery could cause a 36% reduction in cell viability (Figure 23). Also, we noticed that cell viability was reduced in Cas9 expression (23% reduction) and mito-sgRN36 delivery (15% reduction), indicating the cell toxicity could already occur from the Cas9 system without being imported into the mitochondria.

To understand whether the mitochondrial translocation of mito-Cas9 system could cause additional stress on mitochondria. We performed Mito Stress Test to evaluate the influence of mito-Cas9 expression and mito-sgRNA delivery on mitochondria respiration (Figure 24). We utilized the Seahorse XFe96 analyzer to obtain the oxygen consumption rate profile of the cells transfected with mito-Cas9 and mito-sgRNA respectively. The oxygen consumption rate profile represented the mitochondria condition of the cells and different parameters, such as basal respiration, ATP production, proton leak, maximal respiration, and non-mitochondrial respiration could be interpreted (Figure 25). The results showed that mito-Cas9 expression in HeLa cells led to a decreased basal mitochondrial respiration and ATP production compared to control cells (Figure 26A, B), indicating the mitochondrial import of mito-Cas9 caused

additional stress that impaired the mitochondria function. Taken the results of WST-1 assay and Mito Stress Test together, the mito-Cas9 expression in HeLa cells has been verified to impair the mitochondria physiology and cell viability, and the toxicity could come from its mitochondrial translocation and Cas9 protein characteristics.
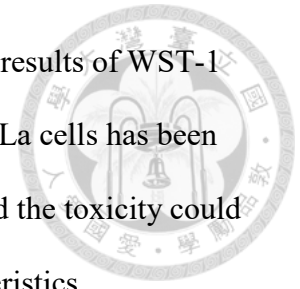
Discussion

1. Previous studies on mtDNA editing by CRISPR-Cas9 system

CRISPR-Cas9 is a popular gene editing technology for nuclear genome editing. However, its application for mitochondrial genome editing were still underdeveloped. Currently, there are five published research about mitochondrial genome editing[24-28]. Jo *et al.*, Loutre *et al.*, Bian *et al.*, and Hussain *et al.* have reported mitochondrial import of Cas9 by a COX8A MTS[24,26,27]. Loutre *et al.* and Hussain *et al.* have used sgRNAs with RNA MTS modifications to transport the sgRNA into mitochondria[25,27]. However, most of these studies did not provide solid evidence of the mitochondria co-localization of both mito-Cas9 and mito-sgRNA. Since the detection of mtDNA depletion can be caused by factors other than Cas9 cleavage of target DNA, such as mitophagy or cell death, lacking evidence for the localization of mito-Cas9 and mito-sgRNA will leave the mtDNA editing results specifically caused by Cas9-induced DNA cleavage questionable.

In order to demonstrate mitochondrial genome editing by CRISPR-Cas9 system, mitochondrial import of Cas9 and sgRNA is essential. The proof of mitochondria co-localization of the mito-Cas9 system is important to validate mito-Cas9 induced DNA cleavage. Also, mitochondria-specific localization can assure the specificity of mito-Cas9 without causing off-target effect on the mitochondrial pseudogenes in the nucleus. On the other hand, the gene toxicity of mito-Cas9 and mito-sgRNA shall be evaluated carefully. In this study, we have pointed out that over-expression of mito-Cas9 and mito-sgRNA can cause negative effects on the cellular system, thereby becomes a hurdle for mtDNA targeting. In short, the construction of a robust mito-Cas9 system requires efficient mitochondria localization and less toxicity to perform precise mtDNA targeting.

2. A novel MTS facilitates mito-Cas9 translocation into mitochondria

In this study, we have tested six different MTSs to facilitate mitochondrial import of Cas9. The MTSs we chose were from proteins with reported mitochondrial translocation activity[24,48-53]. However, most of the MTSs were found to be inefficient for mitochondria translocation of Cas9, including the COX8A MTS that was previously reported to be a suitable MTS for Cas9, as no mitochondria co-localization were observed in these MTS-Cas9 fusion proteins under high resolution confocal microscopy. Only the MTHFD1L MTS was found to be guiding Cas9 into the mitochondria efficiently. The results indicate that the construction of mito-Cas9 requires a specific MTS that can originally facilitate nuclear-encoded large mitochondrial proteins into the mitochondria. Although we have found a MTS for efficient Cas9 import into mitochondria, we also noticed the translocation efficiency could be affected by the expression amplitude. As the mito-Cas9 expression was over-expressed, it could begin to aggregate in the cytosol instead of within mitochondria. Moreover, the mito-Cas9 expression could cause abnormality of the cells over time. These results indicate that it is important to fine-tune mito-Cas9 expression that allows the appropriate amplitude of gene expression for robust mtDNA targeting.

3. Efficient mito-Cas9 gene expression requires optimized approaches

The gene delivery efficiency is a critical factor for operating evaluations of the mito-Cas9 system. We have tested different gene delivery approaches including transfection techniques and lentiviral transduction for mito-Cas9 expression in HeLa cell line. By lipofection, we achieved a 40% gene delivery efficiency with 70% viability. Although transfection efficiency of the large mito-Cas9 plasmid (over eight kilo-base) can have

its limit to reach nearly 100%, we suggest it is feasible to perform transfection efficiency over 40% by lipofection, based on our current data. However, this will require the increase of lipofectamine usage, which may cause additional cellular stress. By lentiviral transduction, we noticed that the doxycycline-inducible system was inefficient for mito-Cas9 expression, possibly due to the cellular response that restricted mito-Cas9 expression.

Also, we constructed a mito-Cas9-P2A-PAC gene expression system to enrich the mito-Cas9 positive cell population by puromycin selection. By delivering the expression system by lipofection, we observed successful enrichment of HeLa cells with mito-Cas9 expression. However, we noticed that the mito-Cas9 expression could still be suppressed throughout cell development. We have not been able to demonstrate the mechanism of the suppression of mito-Cas9, yet we suggest it is most likely by a post-translational mechanism since the gene existence at DNA level in the cells was confirmed by PCR and the puromycin resistance is remained. This finding indicated that not only the over-expression of mito-Cas9 could be a problem, but also the cellular response to counter mito-Cas9 expression became a hindrance for mtDNA targeting.

We evaluated the influence of mito-Cas9 expression on cell viability and mitochondrial stress and verified that mito-Cas9 toxicity could cause reduced cell viability and mitochondrial respiration. Based on our experimental results, we suggested that the mito-Cas9 was toxic because of two factors, the Cas9 protein portion that caused cellular toxicity and the MTS portion that caused mitochondria toxicity by importing Cas9 into the mitochondria.

Challenging as it may be, there are still other approaches worth trying, such as promoter optimization, linearized DNA, or mRNA expression, to expand the time span

suitable for mtDNA editing by mito-Cas9 with reduced toxicity caused by mito-Cas9 expression.
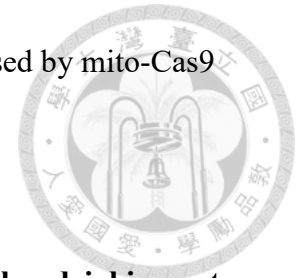
4. Mito-sgRNA with linker modification showed enhanced mitochondrial import efficiency

For sgRNA import into the mitochondria, we have tested 15 mito-sgRNAs with different RNA MTS sequences modified on the sgRNA. Interestingly, the mito-sgRNA that had the highest mitochondrial import efficiency, mito-sgRNA51, was the mito-sgRNA with linker modification instead of other mito-sgRNAs with reported RNA MTS modifications. As we used the RNAfold web tool to predict the mito-sgRNA secondary structure, we found that the linker-modified mito-sgRNA has formed an additional loop structure based on the linker sequence. This additional structure could be the explanation for the enhancement of mitochondrial import as if it be recognized as an RNA MTS by the mitochondrial RNA import pathways. Since the DNA cleavage activity of mito-sgRNAs were also confirmed in our *in vitro* assay, we expect that it is likely the mito-Cas9 and mito-sgRNA can form a RNP complex with endonuclease activity to target mitochondrial genome as they localize within mitochondria.

5. Mito-sgRNA interferes with mtDNA level within mitochondria

While trying to perform mtDNA targeting, we discovered that mito-sgRNA could cause a reduced mtDNA level in HeLa cells as we transfected *in vitro* transcribed mito-sgRNA by lipofection. This is a negative effect in attempt to perform mtDNA targeting by the mito-Cas9 system. The effect could be caused by sequence homology between mtDNA and mito-sgRNA that led to interference of mtDNA replication as the mito-sgRNA anneals with the mtDNA target site. Since the mtDNA reduction was also seen

23

in mito-sgRNA with inefficient mitochondrial translocation efficiency (mito-sgRNA36), another explanation could be the mito-sgRNA interference on cytosolic RNA levels that caused cellular disorders which included mitochondria malfunctioning.

From the WST-1 assay results, we noticed that mito-sgRNA delivery was a stressor that led to a decreased cell viability. This indicates that mito-sgRNA can also cause cellular toxicity. To address this negative effect, other mito-sgRNA expression strategy shall be carried out to evaluate whether the mito-sgRNA toxicity can be ameliorated such as plasmid expression of mito-sgRNA.

6. Perspectives on mtDNA targeting by mito-Cas9 system

In this study, the evidences of mitochondrial translocation of mito-Cas9 and mito-sgRNA have provided a promising foundation for mitochondrial genome editing. However, it was observed that the mito-Cas9 and mito-sgRNA expression in cells could be toxic and became challenging impediments for mtDNA targeting. The current problems in mito-Cas9 expression is that over-expression can cause cellular abnormality and long-term expression leads to gene suppression of mito-Cas9. As for mito-sgRNA, transfection of *in vitro* transcribed RNA causes gene toxicity and reduces the mtDNA. To overcome these problems, different expression strategies are worth trying. For example, the mito-Cas9 expression driven by a weaker promoter may extend the time span of effective mito-Cas9 expression with less toxicity. The plasmid expression of mito-sgRNA may be a better approach instead of IVT RNA transfection in order to allow a suitable amount of mito-sgRNA gradually expressed in cells. As the negative cellular effects can be ameliorated, we expect to establish a robust mito-Cas9 system that can be applied for mitochondrial genome research as well as therapeutic strategies on mitochondria-genetics-related diseases.

Materials and Methods
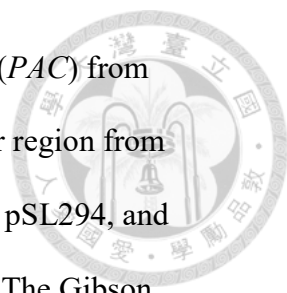
1. Cell culture

HeLa cells were grown in Dulbecco's modified Eagle medium (DMEM) supplemented with 10% heated fetal bovine serum (FBS, 56°C for 30 minutes), 1X Antibiotic-Antimycotic (Thermo Fisher Scientific) and 1% HEPES (v/v) and incubated at 37°C in a humidified atmosphere with 5% CO_2/95% air. For cell passaging, as cell confluency reached 80% in 10-cm plate, the medium was replaced with 5 ml Dulbecco's Phosphate Buffer Saline (DPBS) to wash the cells. Then, 1 ml 0.25% trypsin was added before a 37°C incubation for 3 minutes. After incubation, 3 ml DMEM was added to the cells. The cells were completely detached from the surface with pipetting. 3ml of the cell culture was removed from the plate to leave one-fourth of the cells for reattachment and proliferation at 37°C.

2. Plasmid construction

To construct plasmids used in this study, the reagents including BbsI enzyme, T4 polynucleotide kinase, T4 ligase, and HiFi DNA Assembly Master Mix were purchased from New England Biolabs and used according to the manufacturer's protocol. After plasmid construction, heat-shock transformation was performed to transform the plasmid into competent cells (homemade TOP10 or Stbl3). After 37°C incubation overnight, the plasmid was extracted from the competent *E. coli* cells via ZR Plasmid Miniprep Classic Kit (Zymo Research) according to the manufacturer's protocol. Then, DNA sequencing of the plasmid was performed at the DNA sequencing core facility in Institute of Biomedical Sciences, Academia Sinica.

The plasmid construction of pSL240 and pSL241 was based on Gibson assembly of four PCR amplicons. For pSL240 construction, primer pair SL759 and SL752 were

used to amplify the lentiviral vector with puromycin resistance gene (*PAC*) from pSL141, SL753 and SL754 were used to amplify the hPGK promoter region from pSL141, SL755 and SL756 were used to amplify the *cas9* gene from pSL294, and SL757 and SL758 were used to amplify the *P2A* gene from pSL486. The Gibson assembly was performed by combining 200 ng *PAC* amplicon, 30 ng hPGK protmoter amplicon, 200 ng *cas9* amplicon, 20 ng *P2A* amplicon, and equal volume of 2X HiFi DNA Master Mix followed by 50°C incubation for 1 hour. After Gibson assembly, the pSL240 construct was transformed into homemade TOP10 competent cells. For pSL241 construction, primer pair SL759 and SL752 were used to amplify the lentiviral vector with puromycin resistance gene (*PAC*) from pSL141, SL753 and SL754 were used to amplify the hPGK promoter region from pSL141, SL760 and SL756 were used to amplify the mito-*cas9* gene from pSL295, and SL757 and SL758 were used to amplify the *P2A* gene from pSL486. The Gibson assembly was performed by combining 200 ng *PAC* amplicon, 30 ng hPGK protmoter amplicon, 200 ng *mito-cas9* amplicon, 20 ng *P2A* amplicon, and equal volume of 2X HiFi DNA Master Mix followed by 50°C incubation for 1 hour. After Gibson assembly, the pSL240 construct was transformed into homemade Stbl3 competent cells.

3. Lipofection

For small scale lipofection, 4×10^5 HeLa cells were seeded in a 12-well plate the day prior to transfection. The plasmid DNA (4 ug) was transfected by Lipofectamine 3000 Reagent (Thermo Fisher Scientific) according to the manufacturer's instructions. Accordingly, 4 ul Lipofectamine 3000 was added with 46 ul Opti-MEM (Thermo Fisher Scientific) in a 1.5 ml tube. 4 ug plasmid was added with 8ul P3000™ Reagent (Thermo Fisher Scientific) and Opti-MEM to 50 ul as final volume in another 1.5 ml

tube. Then, the two solutions were combined and incubated at room temperature for 15 minutes. After the incubation, the DNA-lipid complex was added to the cells.
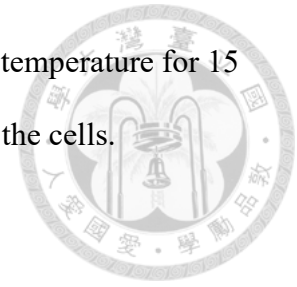
4. Nucleofection

For small scale nucleofection, 2×10^5 HeLa cells were mixed with 20 ul Electroporation Buffer and indicated plasmid DNA (0.5ug-8ug pSL295). The solution was transferred into 16-well 20 ul Nucleovette^{TM} Strip and nucleofected by 4D Nucleofector^{TM} X Unit (Lonza) with program CN-114. After nucleofection, 100 ul DMEM was added into each well for cell recovery at 37°C for 10 minutes. Then, the cells were transferred into 35-mm glass bottom dish (#81158, ibidi) with 1 ml pre-warmed DMEM at 37°C.

5. Immunofluorescence

2×10^5 HeLa cells were seeded in 35-mm glass bottom dish (#81158, ibidi) with 1 ml DMEM. After 48 hours, the cells were washed with 1 ml DMEM. Then, 200 ul 200 nM MitoTracker Deep Red (Invitrogen) in DMEM was added for 30-minute incubation at 37°C. After mitochondria staining, the cells were washed with 1 ml DMEM and incubated at 37°C for 6 hours in 1 ml DMEM. After the incubation, the cells were washed 3 times with 1 ml DMEM before fixation. For cell fixation, 1 ml 4%(w/v) formaldehyde in PBS was added for 15-minute incubation at room temperature. The cells were washed 3 times with 1 ml DPBS and penetrated with 1 ml 0.1% (v/v) Triton X-100 in PBS at room temperature for 15 minutes. After washing the cells 3 times with 1 ml DPBS, the cells were incubated with 200 ul rabbit anti-FLAG antibody (Proteintech; 1:1000 dilution in PBS) at 4°C overnight. The overnight incubation and the following incubations were all under aluminum covering. The overnight samples
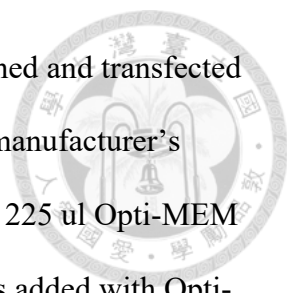
were washed 3 times with 1 ml PBST and once with 1 ml PBS. Then, the cells were incubated with goat anti-rabbit antibody IgG antibody conjugated with Alex Fluor 546 (#A-11035, Thermo Fisher Scientific; 1:2000 dilution in PBS) at room temperature for 30 minutes. The secondary antibody was removed and 200 ul 300 nM DAPI (#D1306, Invitrogen) in PBS was added for 5-minute incubation at room temperature. The samples were washed 3 times with 1 ml PBST and immersed in 1 ml PBS. Then, the samples were imaged under confocal microscopy (Leica SP5 X inverted).

6. Flow cytometry

The HeLa cells in 35-mm glass bottom dish (#81158, ibidi) were washed with 1 ml DPBS and incubated at 37°C for 3 minutes after adding 200 ul 0.25% trypsin. The cells were transferred into 1.5 ml Eppendorf Tube and centrifuged at 300 x g for 3 minutes. After removal of the supernatant, the cell pellet was washed once with 1 ml DPBS and centrifuged at 300 x g for 3 minutes. The supernatant was removed and 100 ul Zombie Violet^{TM} dye (BioLegend; 1:1000 dilution in PBS) was added to the cells. After 15-minute incubation at room temperature under aluminum covering, 1 ml FACS Buffer was added to the cells. The cells were centrifuged at 300 x g for 3 minutes and the supernatant was removed. 1 ml FACS Buffer was added for resuspension, and the cells were transferred to Falcon 5ml Round Bottom Polystyrene Test Tube with Cell Strainer Snap Cap (#352235, Corning). The cell viability and GFP expression were analyzed by Flow cytometer (Beckman Coulter CytoFlex).

7. Stable cell line construction via lentiviral transduction

To produce lentiviral particles for transduction, 1×10^6 Lenti-X 293T cells were seeded in 6-cm plate the day prior to transfection. The plasmid mixture, 2.25 ug pCMV-

ΔR8.91, 0.25 ug pMD.G, and 2.5ug mito-Cas9 plasmid, were combined and transfected by Lipofectamine 2000 (Thermo Fisher Scientific) according to the manufacturer's instructions. Accordingly, 25 ul Lipofectamine 2000 was added with 225 ul Opti-MEM (Thermo Fisher Scientific) 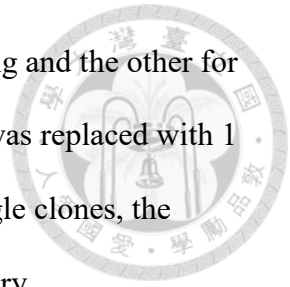in a 1.5 ml tube. The plasmid mixture was added with Opti-MEM to 250 ul as final volume in another 1.5 ml tube. Then, the two solutions were combined and incubated at room temperature for 15 minutes. After the incubation, the DNA-lipid complex was added to the cells. After 37°C incubation for 24 hours, the cell medium was replaced with 5ml DMEM with 1% BSA for lentivirus harvesting. After 24 hours of 37°C incubation, the cell medium containing lentivirus was harvested and stored at 4°C. Meanwhile, 5 ml DMEM with 1% BSA was added to the cells for second harvesting. The next day, the cell medium was harvested and combined with the first harvest. The combined harvest was centrifuged at 500 g for 10 minutes to remove the cell pellet. After the centrifugation, the supernatant was transferred to a 15 ml tube and 3 ml lenti-X concentrator was added for lentivirus precipitation at 4°C overnight. Then, 1500 g centrifugation was performed at 4°C for 45 minutes. The supernatant was removed and the lentivirus pellet was re-suspended with 1 ml DMEM. Before the usage of lentivirus solution for transduction, the solution was stored at -80°C.

1.5×10^5 HeLa cells were seeded in a 12-well plate the day prior to lentiviral transduction. After 24 hours, the cell medium was replaced with 800 ul lentivirus solution containing 8 ug/ml polybrene. After a 37°C incubation overnight, the solution was replaced with 1 ml DMEM with 2ug/ml puromycin. After 48 hours of puromycin selection, the cell medium was replaced with 1 ml DMEM for 24 hours of 37°C incubation. The next day, single cell sorting was performed at the flow cytometry core facility in Institute of Biomedical Sciences, Academia Sinica. The single clones were incubated at 37°C for 3 weeks for cell proliferation. Then, each proliferated single clone

29

was spread to two 96-well plate, one for doxycycline induction testing and the other for doxycycline induction rate analysis. The next day, the cell medium was replaced with 1 ug/ml doxycycline. After confirmation of doxycycline-inducible single clones, the induction rates of those single clones were analyzed by flow cytometry.

8. Stable cell line construction via plasmid transfection

4×10^5 HeLa cells were seeded in 12-well plate the day prior to transfection. The mito-Cas9 plasmid (4 ug) was transfected by Lipofectamine 3000 Reagent (Thermo Fisher Scientific) according to the manufacturer's instructions. Accordingly, 4 ul Lipofectamine 3000 was added with 46 ul Opti-MEM (Thermo Fisher Scientific) in a 1.5 ml tube. 4 ug plasmid was added with 8ul P3000™ Reagent (Thermo Fisher Scientific) and Opti-MEM to 50 ul as final volume in another 1.5 ml tube. Then, the two solutions were combined and incubated at room temperature for 15 minutes. After the incubation, the DNA-lipid complex was added to the cells. After 37°C incubation overnight, the cell medium was replaced with 1 ml DMEM with 2ug/ml puromycin. After every 2 days of puromycin selection, the cell medium was removed and 1ml DMEM with 2ug/ml puromycin was re-added to the cells for totally 2 weeks of puromycin selection. Then, the cell medium was replaced with 1 ml DMEM for cell recovery. After 9 days of cell recovery, puromycin selection was performed to validate the puromycin resistance of the cells.

9. *In situ* RNA detection

1×10^5 HeLa cells were seeded on Superfrost Plus slides (Thermo Fisher Scientific) with attached Secure-seals (Thermo Fisher Scientific, 9 mm diameter and 0.8 mm deep) in 50 ul DMEM. After incubation at 37°C for 24 hours, the cells were fixed with 50 ul

4% (w/v) formaldehyde in PBS for 30 minutes at room temperature. After fixation, the cells were washed 2 times with 50 ul DEPC-treated PBS and dehydrated through a series of 50 ul 70%, 85%, and 99.5% ethanol for 3 minutes each. 50 ul 0.1 M HCl was applied to the cells for 10 minutes at room temperature to make the RNA more readily available for cDNA synthesis. Then, the cells were washed with 50 ul DEPC-PBS for 2 times and preincubated in 50 ul M-MuLV reaction buffer (Thermo Fisher Scientific). The following molecular reactions are all performed in a 50 ul volume.

For cDNA synthesis, 1 uM cDNA primer was added to the cells with 20 U ul^{-1} RevertAid H Minus M-MuLV reverse transcriptase (Thermo Fisher Scientific), 500 nM dNTPs (Promega Corporation), 0.2 ug ul^{-1} BSA (Promega Corporation) and 1 U ul^{-1} RiboLock RNase Inhibitor (Thermo Fisher Scientific) in the M-MuLV reaction buffer (Thermo Fisher Scientific). After incubation at 37°C overnight, the cells were washed with 50 ul PBST (0.1% Tween-20 in PBS), followed by a post-fixation step with 4% (w/v) formaldehyde in PBS for 30 minutes at room temperature. After post-fixation, the cells were washed 2 times in PBST and preincubated in Ampligase buffer (20 mM Tris-HCl, pH 8.3, 25 mM KCl, 10 mM MgCl$_2$, 0.5 mM NAD, and 0.01% Triton X-100).

For padlock probe hybridization, the RNA portion of the created RNA-cDNA hybrids was degraded with ribonuclease H. The RNA degradation was performed in the same step as the padlock probe hybridization and ligation. The padlock probes were 5'-phosphorylated at a concentration of 2 uM with 0.2 U ul^{-1} T4 polynucleotide kinase (New England Biolabs) and 1 mM ATP in the manufacturer's buffer for 30 minutes at 37°C, followed by 10 minutes at 65°C. Then, 100 nM padlock probe with 0.5 U ul^{-1} Ampligase (Lucigen), 0.4 U ul^{-1} RNaseH (New England Biolabs), 1 U ul^{-1} RiboLock RNase inhibitor (Thermo Fisher Scientific), 50 mM KCl, and 20% formamide in Ampligase buffer were added to the cells. Incubation was performed at 37°C for 30

minutes, followed by 45°C for 45 minutes. The cells were preincubated in **Φ29 DNA**

polymerase buffer (Thermo Fisher Scientific).

For rolling circle amplification (RCA), 1 U ul^{-1} **Φ29 DNA polymerase** (Thermo Fisher

Scientific) with 1U ul^{-1} RiboLock RNase Inhibitor (Thermo Fisher Scientific), 250 uM

dNTPs (Promega Corporation), 0.2 ug ul^{-1} BSA (Promega Corporation), and 5%

glycerol in the supplied reaction buffer were added to the cells. After Incubation at 37°C

for 1 hour, the cells were washed with 50 ul PBST. To visualize the RCA products, 100

nM detection probe and 20% formamide in SSC buffer were added to the cells and

incubated at 37°C for 30 minutes. After incubation, the cells were washed with 50 ul

PBST and dehydrated through a series of 50 ul 70%, 85%, and 99.5% ethanol for 3

minutes each. 50 ul 300 nM DAPI was added to the cells to stain the nuclei. The

Secure-seals were removed and the slides were mounted with Vectashield (Vector).

After covering the cells with a cover glass and sealed with nail polish, the samples were

imaged under confocal microscopy (Leica SP5 X inverted).

10. RNA synthesis by T7 *in vitro* transcription

To synthesize RNA by T7 *in vitro* transcription, 6M urea-polyacrylamide gel with

10% polyacrylamide in a hand-made gel utensil was prepared in advance. Two large

size glass slides were sprayed with nuclease/EtBr terminator (Protech) and cleaned by

tap water. After the glass slides being dried with paper towel, 100 ul of Sigmacote

(Sigma-Aldrich) was added onto one side of each glass and spread out through the glass

surface by Kimwipe for coating. The two glass slides were stacked with 2 spacers (0.3-

cm thickness) in between on opposite edges as the coated side being the inner side.

Three edges were taped with 3M electrical tape leaving the top edge not sealed. The

bottom edge was taped again to strengthen the hand-made gel utensil. Then, 100 ml of
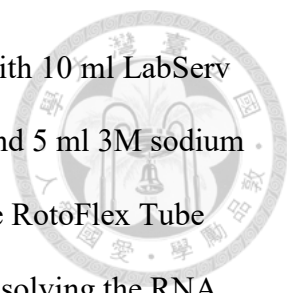
premixed urea gel solution was mixed with 50 ul TEMED and 200 ul 20% APS in a beaker. Right after mixing, the mixture was added into the utensil and a comb was inserted from the top of the gel solution. The urea-gel would be ready for electrophoresis as it solidified.
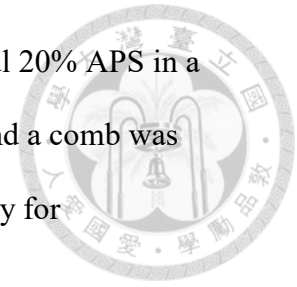
The DNA template for RNA synthesis was prepared by PCR using KAPA HiFi PCR kit (KAPA Biosystems, USA) according to the manufacturer's protocol. After a 60 ul PCR reaction, 3 ul of the product was taken for 2% agarose gel electrophoresis to validate the DNA quality. The remaining 57 ul DNA template was mixed with 30 ul 10X IVT buffer, 60 ul 25 mM NTP, 6 ul dithiothreitol (DTT), 30 ul 50% polyethylene glycol (PEG), 30 ul 100 ug/ml T7 polymerase, and 87 ul DEPC H_2O for a total 300 ul reaction. The mixture was incubated at 37°C for 2 hours to transcribe the RNA. Then, 1ul of RQ1 RNase-free DNase (Promega, Madison, WI) was added to the mixture and incubated at 37°C for 1 hour. After the DNA digestion, 150 ul 2X STOP solution (95% deionized formamide, 0.05% [w/v] bromophenol blue, 0.05% [w/v] xylene cyanol FF, and 20 Mm EDTA, pH 8) was added to the mixture for 10-minute incubation at 50°C.
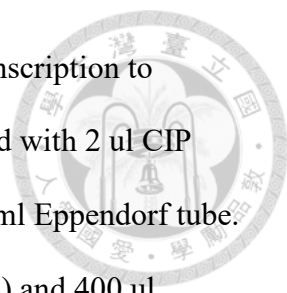
To perform urea-polyacrylamide gel electrophoresis (Urea-PAGE), the 3M electrical tapes on the urea-gel slides were torn off and the slides were set up onto the Owl^{TM} Dual-Gel Vertical Electrophoresis System (Thermo Fisher Scientific). The comb was taken away and the wells were washed by pipetting. After loading the RNA into the wells, electrophoresis was started with a constant 250 mA current by using the EC300XL power supply (Thermo Fisher Scientific) for approximately 4 hours until bromophenol blue reaches the bottom of the gel.

The glass slides were removed after electrophoresis, and the gel was covered with plastic wrap to avoid contamination. The RNA was visualized by a brief UV light and marked out on the plastic wrap. To purify the RNA product, the RNA portion of the gel

33

was excised and transferred to a 50 ml tube. After crushing the gel with 10 ml LabServ Serological Pippette (Thermo Fisher Scientific), 30 ml DEPC H_2O and 5 ml 3M sodium acetate (pH 5) were added to the gel. The 50 ml tube was set onto the RotoFlex Tube Rotator (Argos Technologies) for overnight rotation at 4°C. After dissolving the RNA from the gel, the RNA solution was separated from the gel by 3500 rpm centrifugation at 4°C for 15 minutes with Allegra X-30R centrifuge (Beckman Coulter). The RNA solution was transferred to a new 50 ml tube and thoroughly mixed with 40 ul 1mg/ml glycogen and 25 ml isopropanol. Then, the RNA was kept at -20°C overnight for precipitation. After RNA precipitation, centrifugation with 4000 rpm at 4°C for 15 minutes was performed to collect the RNA pellet. The supernatant was removed yet leaving 1 ml to re-suspend the RNA. The RNA resuspension was transferred to a 1.5 ml Eppendorf tube and underwent 14000 rpm centrifugation at 4°C for 1 minute with Centrifuge 5424R (Eppendorf). The supernatant was removed and the RNA pellet was washed three times with 1 ml 70% ethanol followed by washing once with 1ml 100% ethanol. After washing, the tube was put into the Centrifugal evaporator CVE-2100 (EYELA) at room temperature for a 10-minute operation to dry the RNA pellet. The pellet was dissolved with 80 ul RNA dissolving buffer (20 mM HEPES [pH 7.5], 150 mM KCl, 10% glycerol, and 1 mM TCEP). The tube was briefly spun down and the supernatant was transferred to a new 1.5 ml Eppendorf tube to exclude unexpected gel debris. After the measurement of the RNA concentration with Nanodrop Lite spectrophotometer (Thermo Fisher Scientific), the RNA was frozen by liquid nitrogen and stored at -80°C.

11. Calf intestinal alkaline phosphatase (CIP) treatment

CIP treatment was applied to the RNA synthesized by *in vitro* transcription to remove the phosphate group on the 5' end. 600 pmol RNA was added with 2 ul CIP (New England Biolabs) and RNA dissolving buffer to 30 ul in a 1.5 ml Eppendorf tube. After 1 hour incubation at 37°C, 370 ul 20 mM sodium acetate (pH 5) and 400 ul phenol: chloroform (low pH) were added to the tube and mixed thoroughly by vortex. Then, 21130 g centrifugation at 4°C for 15 minutes was performed with Centrifuge 5424R (Eppendorf) and the upper layer containing the RNA was transferred to a new 1.5 ml tube. The RNA was mixed thoroughly with 400 ul chloroform followed by 21130 g centrifugation with at 4°C for 15 minutes. The upper layer was transferred to a new 1.5 ml tube and mixed thoroughly with 10 ul 1mg/ml glycogen, 100 ul 3M sodium acetate (pH 5), and 1ml isopropanol for RNA precipitation. After RNA precipitation at -20°C overnight, the RNA pellet was obtained with 16000 g centrifugation at 4°C for 10 minutes. The supernatant was removed and the RNA pellet was washed with 1 ml 70% ethanol for three times followed by washing once with 100% ethanol. After washing, the tube was put into the Centrifugal evaporator CVE-2100 (EYELA) at room temperature for a 10-minute operation to dry the RNA pellet. The pellet was dissolved with 20 ul RNA dissolving buffer (20 mM HEPES [pH 7.5], 150 mM KCl, 10% glycerol, and 1 mM TCEP). After the measurement of the RNA concentration with Nanodrop Lite spectrophotometer (Thermo Fisher Scientific), the RNA was diluted to 10 uM, frozen by liquid nitrogen, and stored at -80°C.

12. RNA transfection

For mito-sgRNA transfection, 3×10^5 cells were seeded in a 6-well plate the day prior to transfection. The mito-sgRNA was heated at 65°C for 5 minutes and cooled down at room temperature for 10 minutes to refold the RNA. After RNA refolding, the mito-

sgRNA was transfected by Lipofectamine 2000 (Thermo Fisher Scientific) according to the manufacturer's instructions. Accordingly, 3 ul Lipofectamine 2000 was added with 197 ul Opti-MEM (Thermo Fisher Scientific) in a 1.5 ml tube. 70 pmol RNA was added with Opti-MEM to 200 ul as final volume in another 1.5 ml tube. Then, the two solutions were combined and incubated at room temperature for 15 minutes. After the incubation, the DNA-lipid complex was added to the cells.

13. DNA extraction

For cellular DNA extraction, 1×10^6 HeLa cells were collected from 6-well plate. Quick-DNA^{TM} Miniprep Plus kit (Zymo Research) were used to extract the genomic DNA according to the manufacturer's instructions.

14. Quantitative real-time polymerase chain reaction (qPCR)

To quantify DNA levels in HeLa cells, qPCR was conducted by Power SYBR Green Master Mix (#4367659, Thermo Fisher Scientific) on the StepOnePlus^{TM} Real-Time PCR system (Applied Biosystems) in triplicate for all samples as following. 2 volumes of SYBR Green was premixed with 1 volume of 1 uM primers. 36 ul of SYBR Green/primers mixture was distributed for each triplicate samples, and 15 ul of the mixture was distributed for no template control in a PCR tube. 12 ul of 10 ng genomic DNA from each sample was added to the tube. 15 ul of the final mixture was distributed into optical tubes with low retention tips. After capping the tubes and cleaning the surface with Kimwipe, the samples were briefly spin down and put into the StepOnePlus^{TM} Real-Time PCR system for qPCR analysis.

15. WST-1 assay

To analyze the cell viability in 96-well plate, 10ul WST-1 reagent (Abcam) was added to each sample. After a 1-hour incubation at 37℃, 5% CO_2 condition, 100 ul medium in each sample was transferred to ELISA 96 well plate. The absorption wavelength of 440 nm was detected, with 660 nm as reference wavelength by the ELISA Reader (Tecan Infinite M1000 Pro).

16. Mito Stress Test

2×10^4 HeLa cells were seeded in Seahorse XF96 Microplate (Agilent) with 80 ul DMEM the day prior to transfection. The surrounding wells on the four edges were added 80 ul DMEM to maintain the humidity of the plate atmosphere. Each detection probe was immersed in 200 ul calibrant within the 96-well utility plate (Aglient) at 37℃ without 5% CO_2 maintenance overnight. The next day, the cell medium was replaced with 180 ul assay medium (DMEM [pH 7.4], 2mM L-glutamine, 2% FBS) in each well and incubated at 37℃ without 5% CO_2 maintenance 1 hour prior assay. The wells with no cells were also containing 180 ul medium. 20 ul 10 uM oligomycin was injected in the A port, 22 ul 10 uM FCCP was injected in the B port, and 25 ul 5uM Rotenone/Antimycin A was injected in the C port of each well of the utility plate with cells. The A, B, and C ports of the wells with no cells were injected the respective volume of medium equal to the volume of the reagents added. Then, the calibration and Seahorse assay were operated by the Seahorse XFe96 Analyzer (Agilent).

17. Statistical analysis

All experimental data were analyzed using Prism 6 software (GraphPad Software, San Diego, CA). Data are reported as mean ± standard deviation. Pairwise comparisons

were analyzed by t-tests. Differences with P value < 0.05 were considered statistically significant.

Figures

Non-programmable	Programmable	
Protein:DNA pairing		RNA:DNA pairing
restriction enzyme	ZFN & TALEN	CRISPR-Cas9
SmaI CCCGGG GGGCCC **XmaI** CCCGGG GGGCCC **ApaLI** GTGCAC CACGTG	FokI FokI	Cas9 Guide RNA
Limited target sites	**Time-consuming construction**	**Efficient targeting**

Figure 1. Gene editing technologies comparison

Restriction enzymes can be efficient for target DNA cleavage, but their limitations on target selection hinders their applicability for gene editing. Artificial DNA endonucleases (ZFN, TALEN) utilized recombinant protein fusing restriction enzyme, FokI, with DNA binding domains for programmable DNA targeting. However, these gene editing technologies require laborious process to design the DNA targets. CRISPR-Cas9 relies on a Cas9 protein with sgRNA to perform gene editing. The simplicity of DNA targeting by changing the guide RNA sequence makes CRISPR-Cas9 an ideal genetic tool.
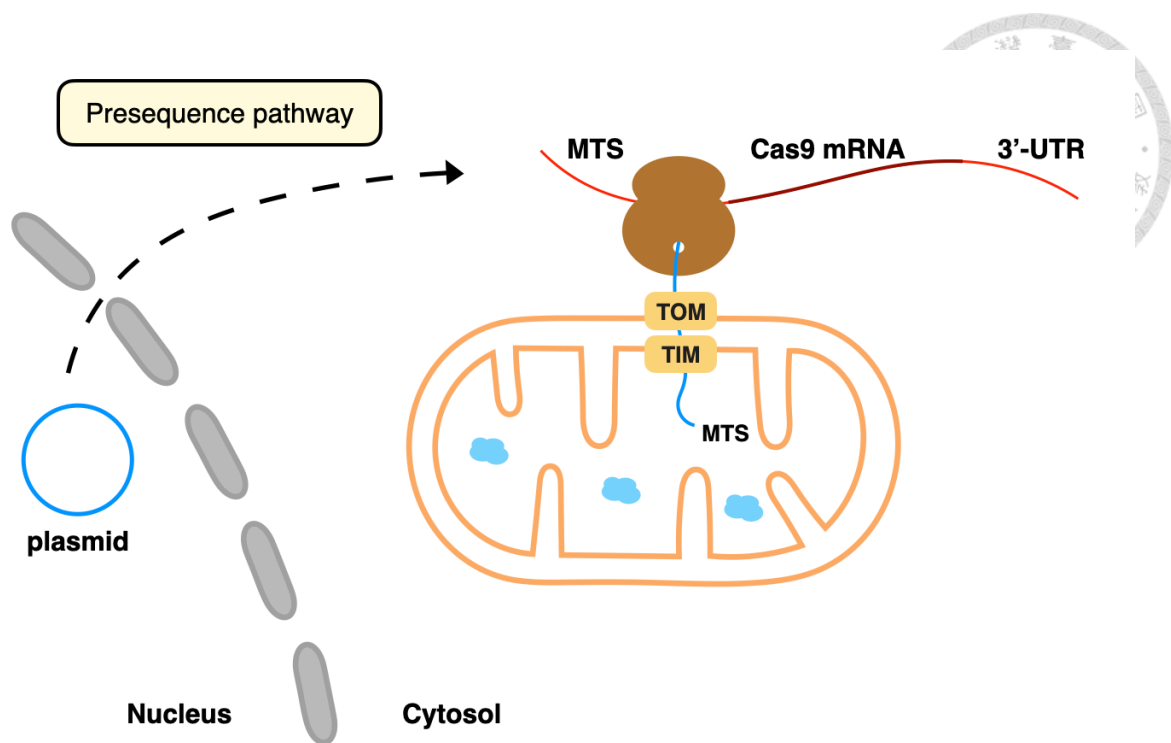
Figure 2. Co-translational mechanism for mitochondrial protein import

The mechanism of mitochondrial protein import into the matrix is during a co-translational process. The transcribed mRNA was guided to the mitochondrial outer membrane facilitated by protein recognition of its 3'-untranlsated region (UTR). As the mRNA started to be translated by the ribosome complex, the polypeptide with mitochondria targeting sequence (MTS) could be recognized by TOM and be transported into the mitochondrial matrix through the TOM-TIM channel. Then, the transported polypeptide could refold into its functional form. Based on this mechanism, we delivered the exogenous Cas9 gene with MTS to allow mitochondrial import through the co-translational process.
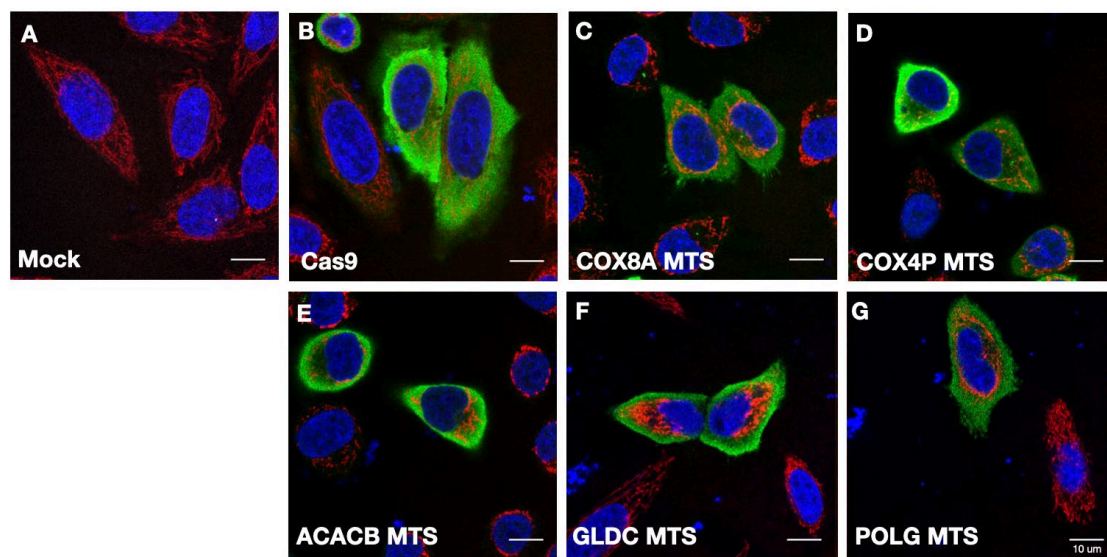
Figure 3. Most MTSs are not suitable for mito-Cas9 construction

Cas9 fusion proteins with several different MTSs have not been found to be imported into the mitochondria. (A) HeLa cells with no treatment. (B) Cas9 without MTS in HeLa cells. (C) Cas9 with double repeats of MTSs from COX8A, 1-21 aa. (D) Cas9 with MTS from S. cerevisiae COX4P, 1-24 aa. (E) Cas9 with MTS from Acetyl-CoA carboxylase 2, 1-40 aa. (F) Cas9 with MTS from mitochondrial glycine dehydrogenase, 1-35 aa. (G) Cas9 with MTS from DNA polymerase gamma-1, 1-38 aa. Blue signal, nuclei stained by DAPI. Red signal, mitochondria stained by MitoTracker Deep Red. Green signal, Cas9 detected by anti-FLAG primary antibody and Alexa Fluor 546-conjugated secondary antibody.
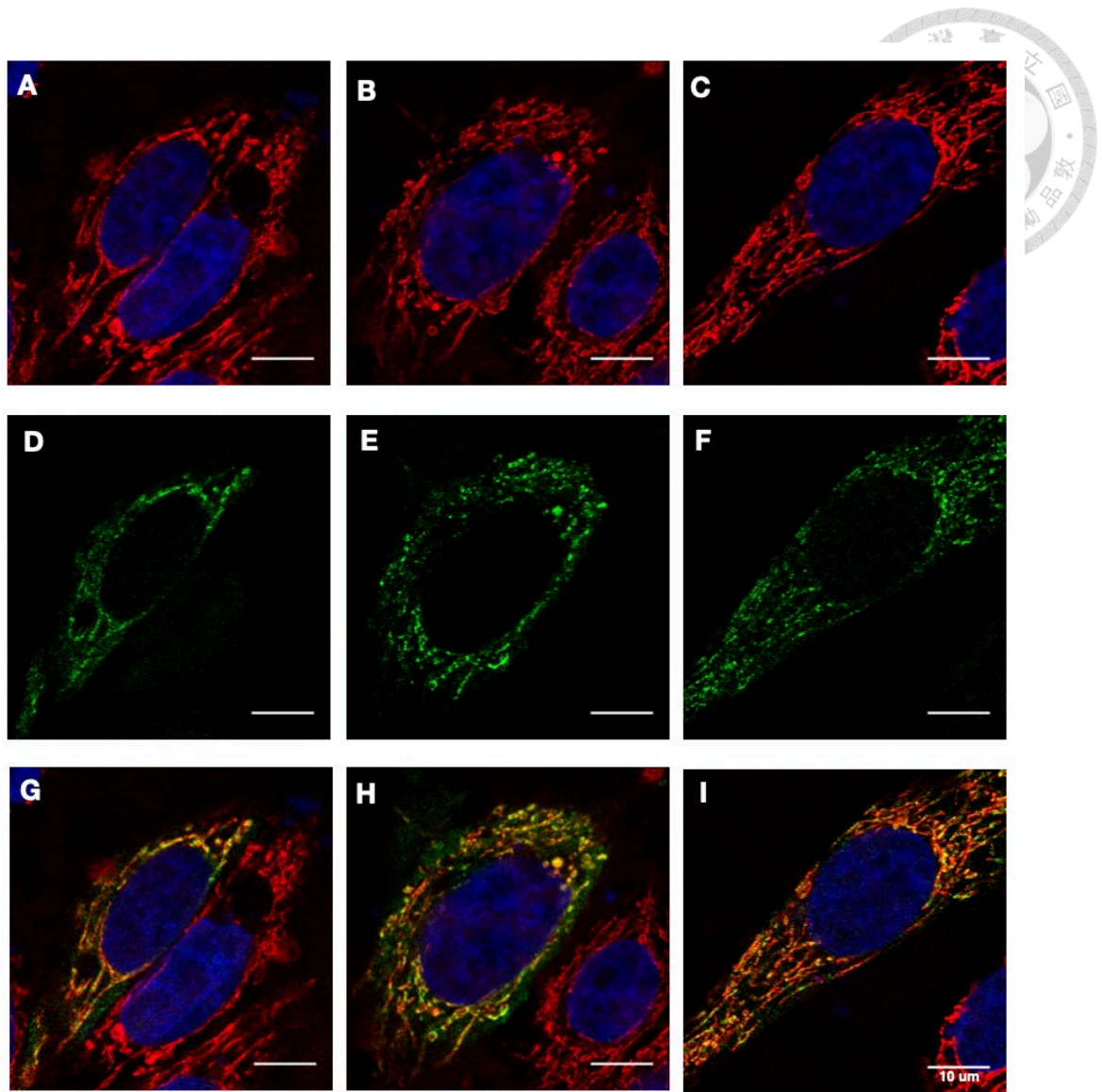
Figure 4. Immunofluorescence images of mito-Cas9

MTS from mitochondrial monofunctional C1-tetrahydrofolate synthase, 1-38 aa, was found to be the efficient MTS for mitochondrial import of Cas9. (A-C) HeLa cells with nuclei stained by DAPI (blue) and mitochondria stained by MitoTracker Deep Red (red). (D-F) HeLa cells with mito-Cas9 detected by anti-FLAG primary antibody and Alexa Fluor 488-conjugated secondary antibody (green). (G-I) Merged images of A-F showed the co-localization of mitochondria and mito-Cas9 (orange).
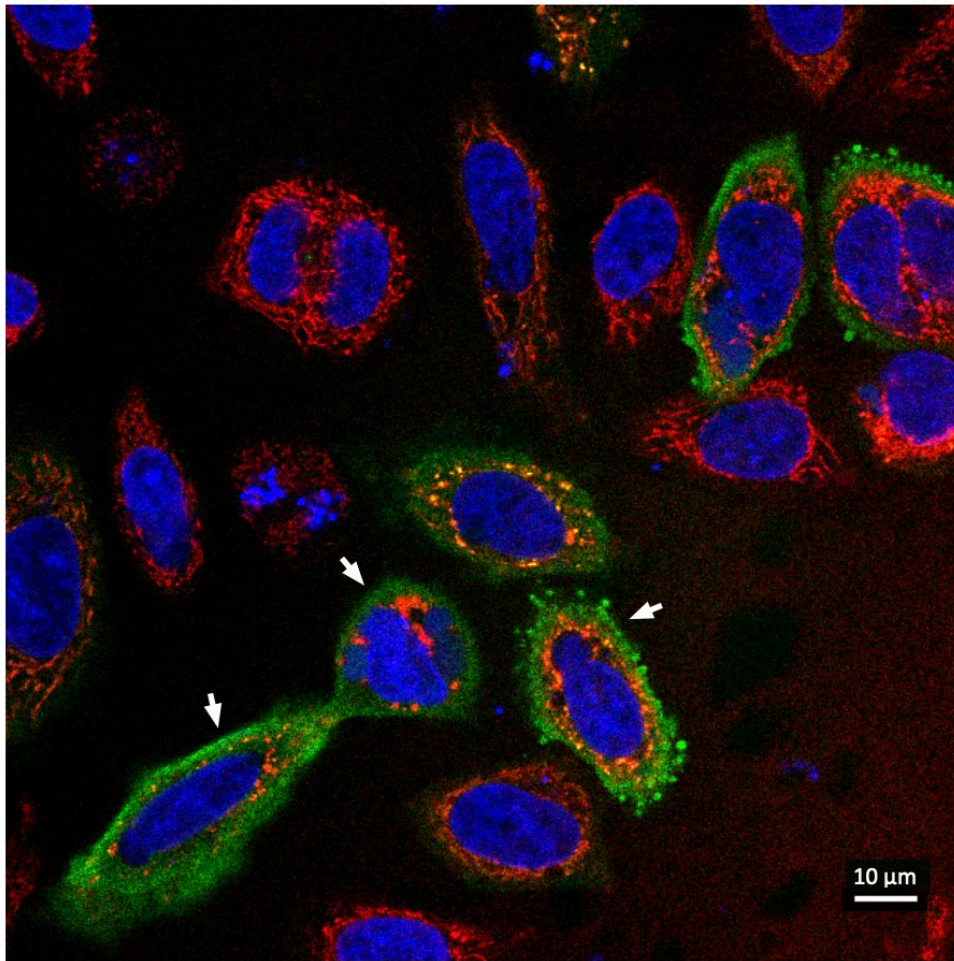
Figure 5. Problems of mito-Cas9 expression

HeLa cells with nuclei stained by DAPI (blue), mitochondria stained by MitoTracker

Deep Red (red), and mito-Cas9 detected by anti-FLAG primary antibody and Alexa

Fluor 488-conjugated secondary antibody (green). The mito-Cas9 over-expression could

cause cell toxicity and loss of mitochondria localization (white arrows).
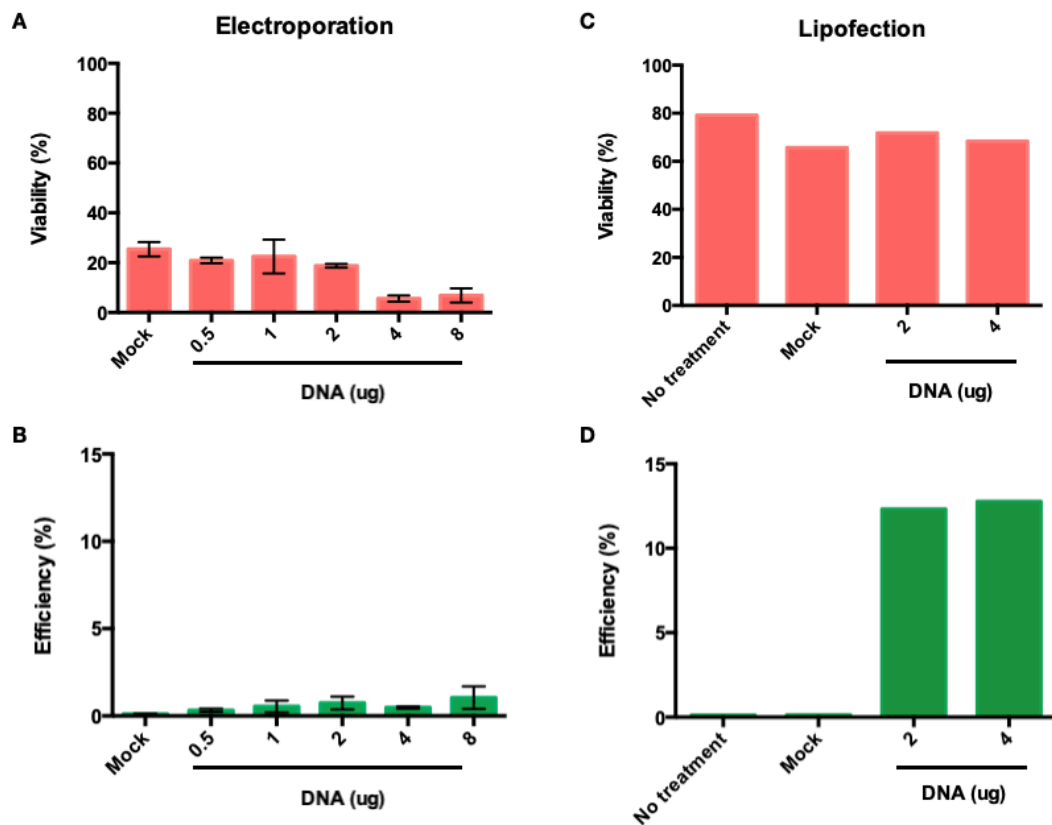
Figure 6. Mito-Cas9 transfection efficiency comparison between lipofection and electroporation

The transfection efficiency of the mito-Cas9-turbo GFP plasmid in HeLa cells was determined by flow cytometry analyzing the GFP signals. The cell viability was determined by staining the dead cells with Zombie violet dye. The overall transfection efficiency was lower than 1% with viability less than 30% for electroporation. On the other hand, the lipofection efficiency can be up to 12% with about 70% viability.
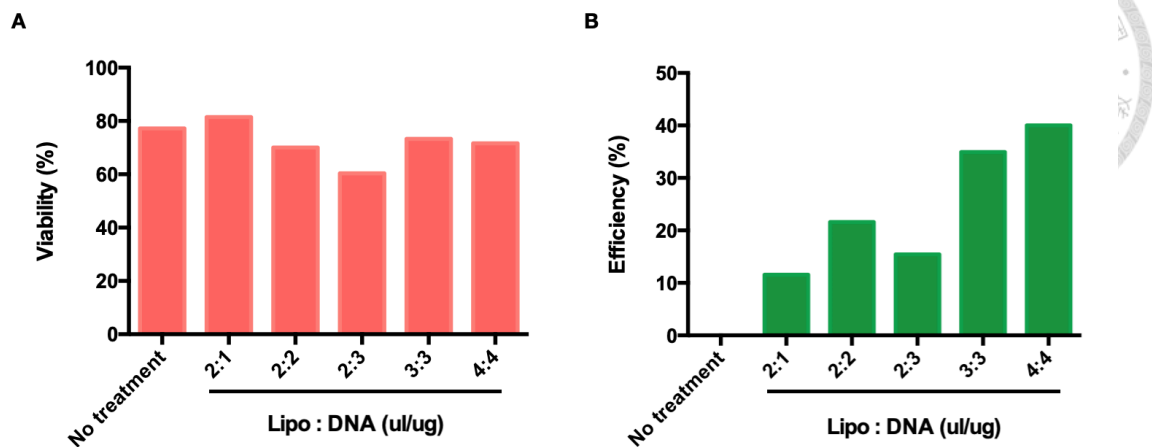
Figure 7. Mito-Cas9 lipofection efficiency optimization in 24-well plate

The lipofection efficiency varies from different ratio of lipofectamine 3000 to plasmid amount. The four microliter lipofectamine 3000 to four microgram plasmid condition could yield a 40% transfection efficiency.
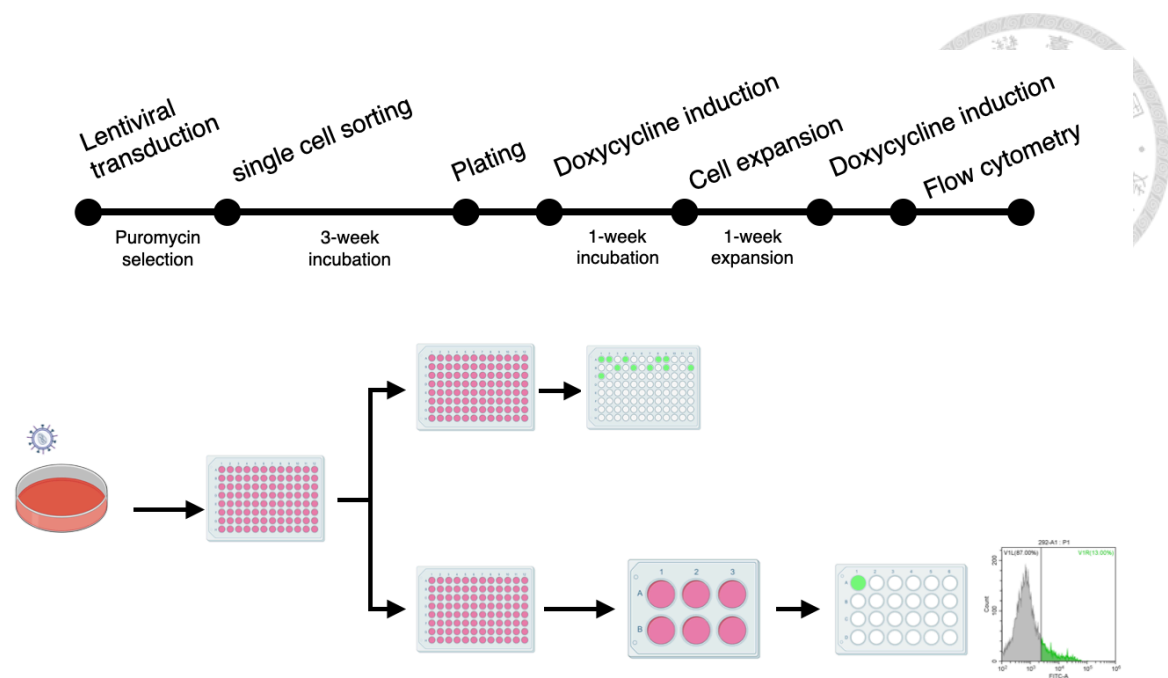
Figure 8. Schematic flow chart for construction of doxycycline-inducible mito-Cas9 stable cell line

To construct an inducible mito-Cas9 cell line in HeLa cells, we performed lentiviral transduction to integrate the inducible mito-Cas9 system into the genome and sorted out the positive cells by puromycin selection followed by single cell sorting. After three weeks for cell expansion, each single clone was transferred to two individual plates. One plate was for inducible clone screening by adding doxycycline to the cells. As the inducible clones were confirmed, the respective clones on the other plate were analyzed of the gene induction rate by doxycycline induction followed by flow cytometry analysis.
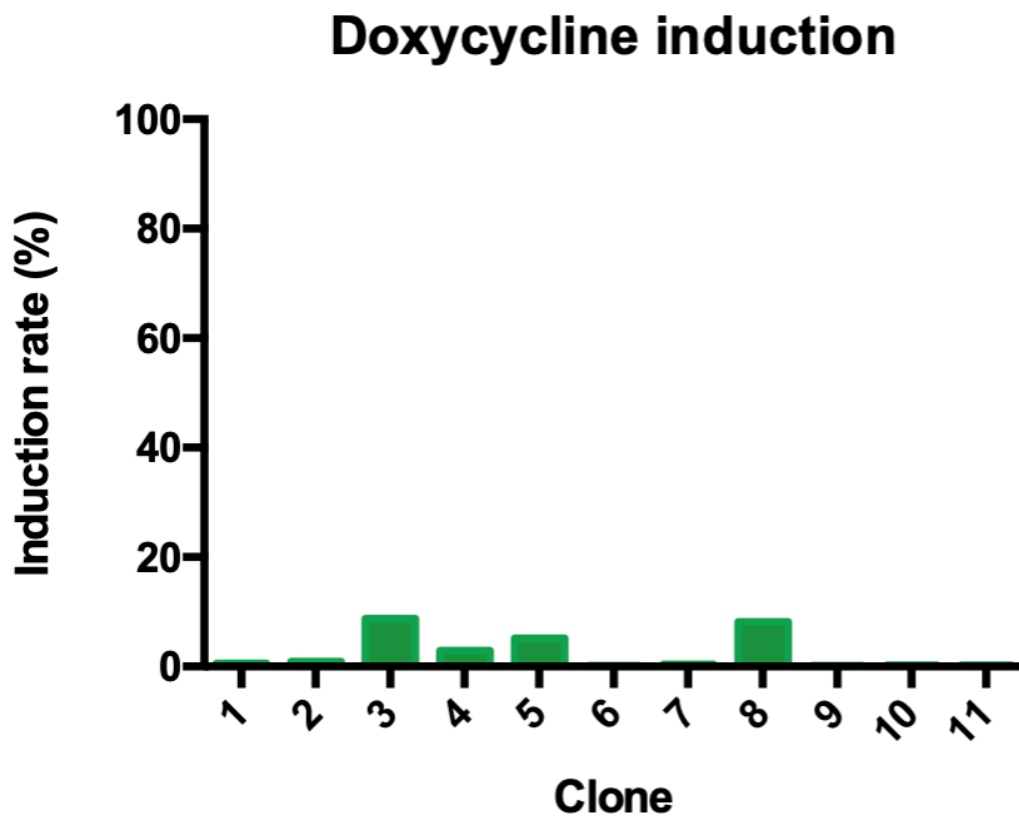
Figure 9. The gene expression rate of mito-Cas9 inducible system in single-clone developed cells

The inducible mito-Cas9 expression in HeLa cells found to be inefficient. The single-clone developed cells that was previously confirmed of the gene integration by puromycin selection and doxycycline induction result in a low induction rate throughout every clone. The highest induction rate among the clones could only be up to 8.72% (clone #3), whereas most of the clones could not express mito-Cas9 for more than 1% in the cell population.
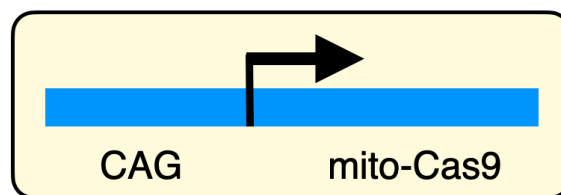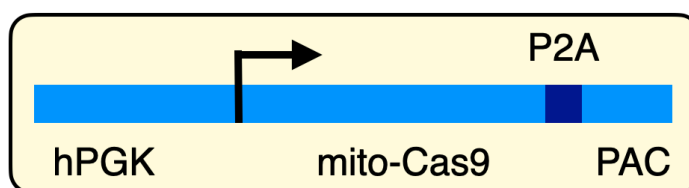
Figure 10. Development of mito-Cas9 expression systems

Since the mito-Cas9 expression encounters cell toxicity and low efficiency problems in previous expression strategies (strategy #1 and #2), we have fine-tuned the mito-Cas9 expression by changing the CAG promoter to an hPGK promoter to lower the strength of gene expression (strategy #3). Moreover, we constructed a mito-Cas9 expression system that utilize the hPGK promoter to drive the puromycin resistance gene (PAC) downstream of the mito-Cas9. This strategy is to assure the mito-Cas9 expression in puromycin-selected cells.
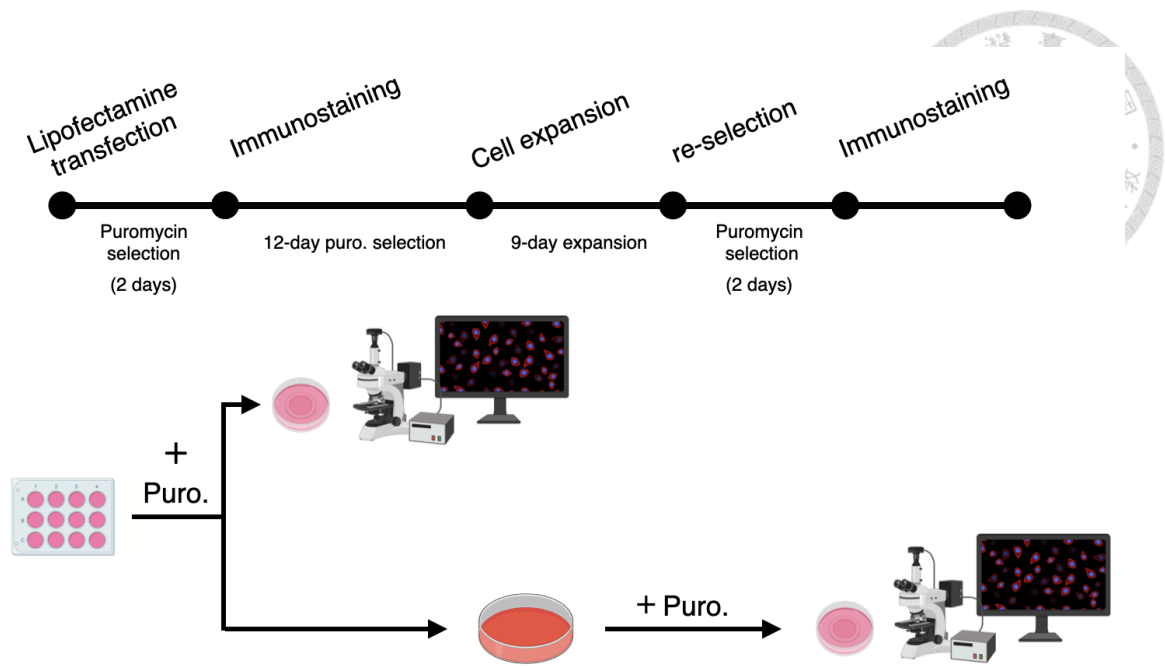
Figure 11. Schematic flow chart for mito-Cas9 cell line preparation via puromycin selection

To evaluate the efficacy of mito-Cas9 expression in the puromycin-selected cells, we transfected the plasmid (pSL241) into HeLa cells using Lipofectamine 3000 reagent and analyzed the gene expression after puromycin selection under confocal microscopy. Also, we continuously incubated the cells in puromycin condition to determine whether this expression system could be maintained in the long term. After three weeks, second gene expression analysis of the cells was performed.

49
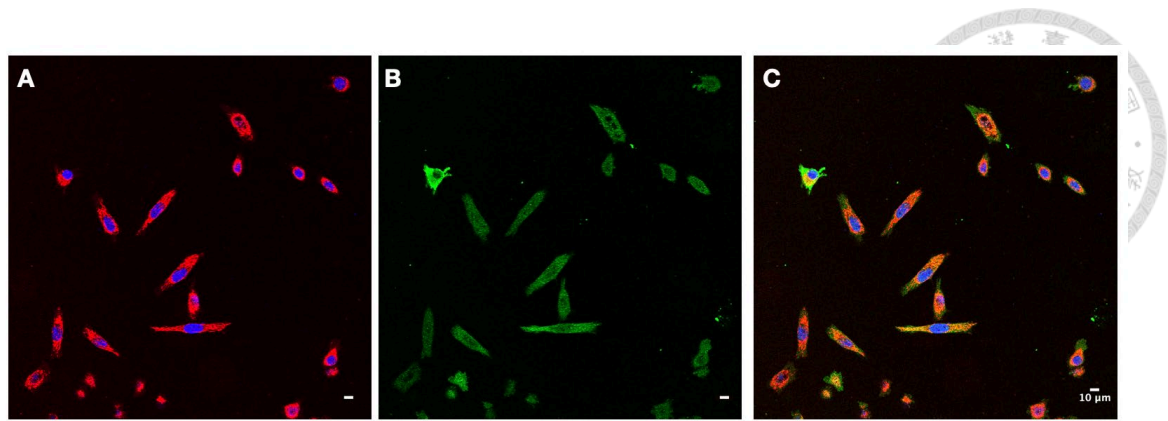
Figure 12. Puromycin selection strategy yield an enriched population of mito-Cas9 positive HeLa cells

The mito-Cas9 expression could be observed in the HeLa cell population after puromycin selection. This expression strategy showed to be efficient for transient mito-Cas9 cell line production. (A) HeLa cells with nuclei stained by DAPI (blue) and mitochondria stained by MitoTracker Deep Red (red). (B) HeLa cells with mito-Cas9 detected by anti-FLAG primary antibody and Alexa Fluor 546-conjugated secondary antibody (green). (C) Merged images of A & B showed the co-localization of mitochondria and mito-Cas9 (orange).
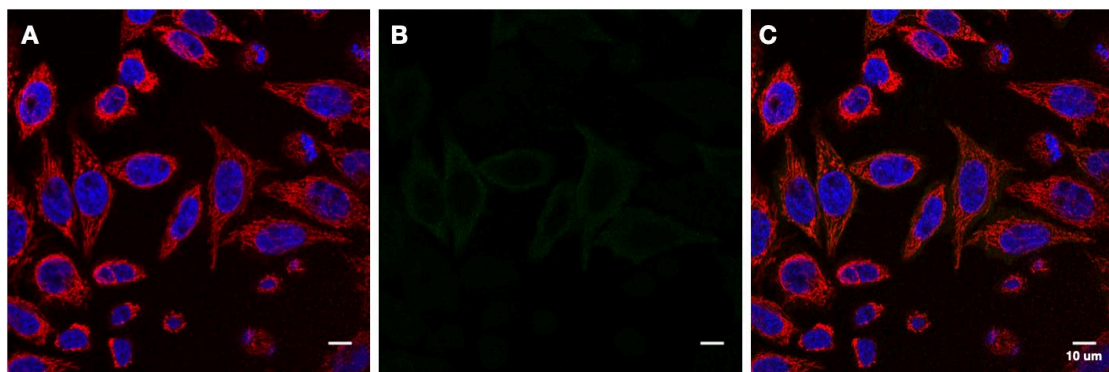
Figure 13. Mito-Cas9 extinction in HeLa cells after a three-week cell development

The puromycin-selection strategy for mito-Cas9 positive cell line preparation were found to be hindered through cell development. The HeLa cells that previously selected by puromycin and confirmed of the mito-Cas9 expression have lost their mito-Cas9 expression while remained puromycin resistant. (A) HeLa cells with nuclei stained by DAPI (blue) and mitochondria stained by MitoTracker Deep Red (red). (B) HeLa cells with mito-Cas9 detected by anti-FLAG primary antibody and Alexa Fluor 546-conjugated secondary antibody (green). (C) Merged images of A & B.
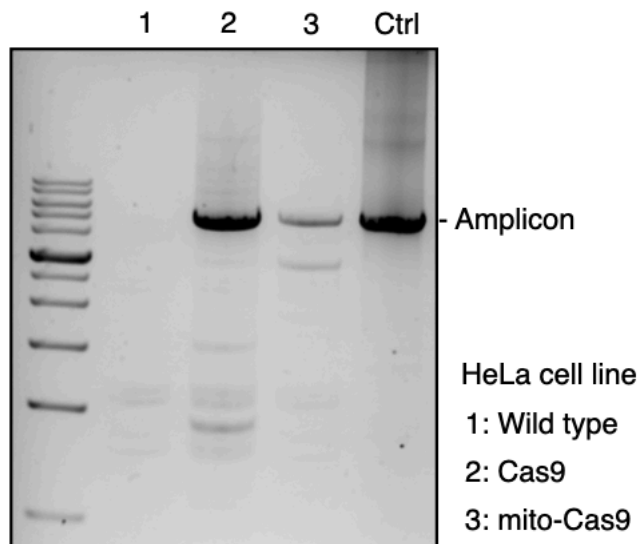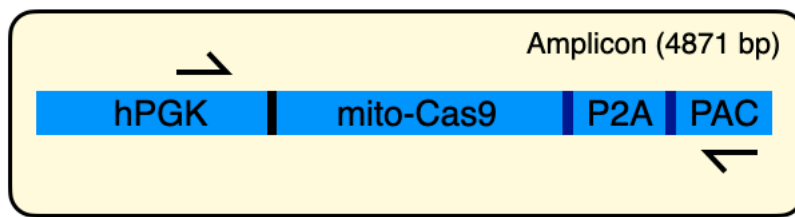
Figure 14. Mito-Cas9 gene expression system remains in HeLa cells after a three-week cell development

The puromycin-resistant HeLa cells that lost their mito-Cas9 expression have kept the mito-Cas9 gene expression system within the cells. We performed PCR analysis to detect the existence of the mito-Cas9 and PAC expression system driven by the hPGK promoter and found that the gene cassette remained in the cellular system after the 3-week cell development. Lane 1: wild type HeLa genomic DNA. Lane 2: Cas9 positive HeLa genomic DNA. Lane 3: mito-Cas9 positive genomic DNA. Control: plasmid of mito-Cas9 expression system.
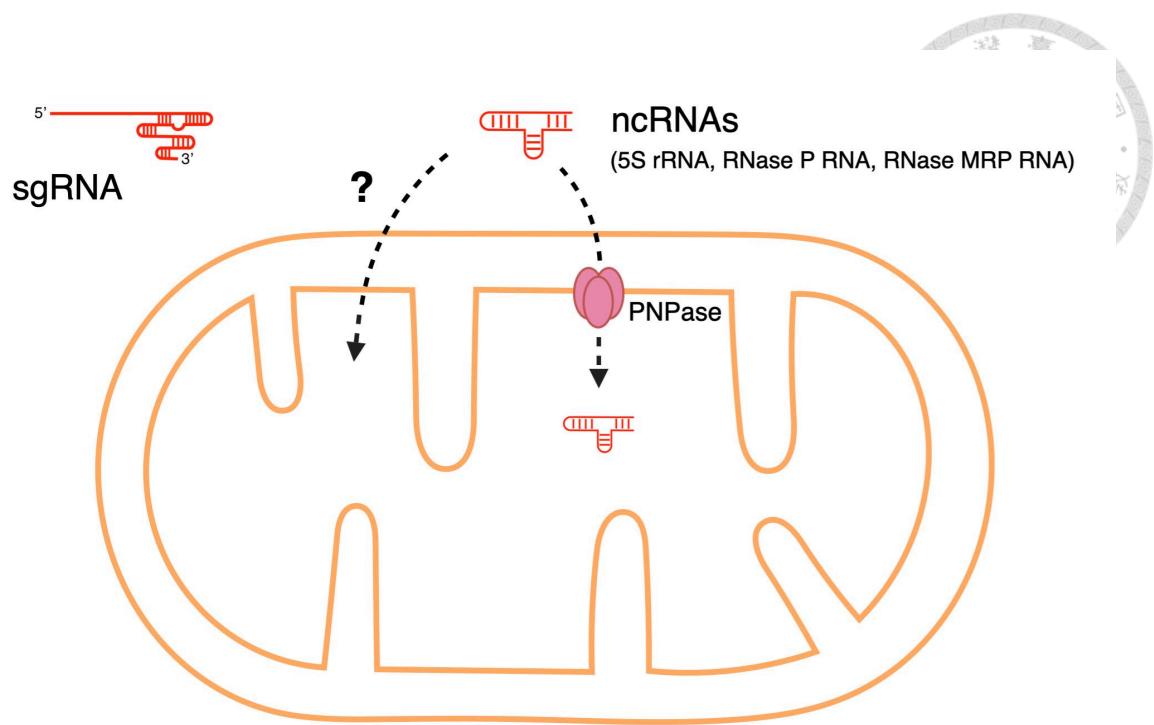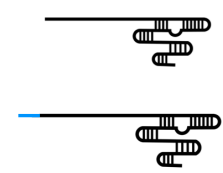
Figure 15. Mitochondrial RNA import mediated by PNPase

Although the mechanism of mitochondrial RNA import is still unclear, studies have reported non-coding RNAs such as 5S rRNA, RNase P RNA and RNase MRP RNA could be transported into the mitochondrial matrix by PNPase recognition. The loss of hairpin-shaped motifs of the ncRNAs would lead to a reduction of these RNAs in the mitochondria. To construct mito-sgRNAs, we modified our sgRNAs with those hairpin-shaped motifs for mitochondrial import.
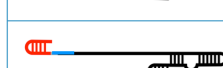
Figure 16. Reported hairpin-shaped motifs for mitochondrial RNA transportation

The hairpin-shaped RNA motifs in this study have been experimentally proven to facilitate RNA import into human mitochondria. (A) Hairpin structure from the gamma domain of 5S rRNA, 65-110 nt. (B) Hairpin structure from the RNase P RNA, 1-20 nt. (C) Hairpin structure from the RNase MRP RNA, 150-169 nt. (D) The double hairpin structure from the F-form of yeast tRNA[Lys]. (E) The hairpin structure from F-form of yeast tRNA[Lys].

Figure 17. Illustration of mito-sgRNA design with predicted secondary structure

We have designed a series of mito-sgRNAs for mitochondrial import. Mito-sgRNA36 is a non-modified sgRNA targeting the ND4 gene on mtDNA. Mito-sgRNA51 is a ND4 targeting sgRNA with a 10-nucleotide linker. Mito-sgRNA52, 53, 56, 68, 73 are ND4 targeting sgRNAs linked with different hairpin-shaped motifs on the 5' end. Mito-sgRNA 69, 70, 71, 72, 74 are ND4 targeting sgRNAs linked with hairpin-shaped motifs in the internal region of the sgRNA scaffold. Mito-sgRNA54, 55, 57 are ND4 targeting sgRNAs linked with hairpin-shaped motifs on the 5' end and modified with 3'-UTR sequence of mitochondrial ribosomal protein S12.

55
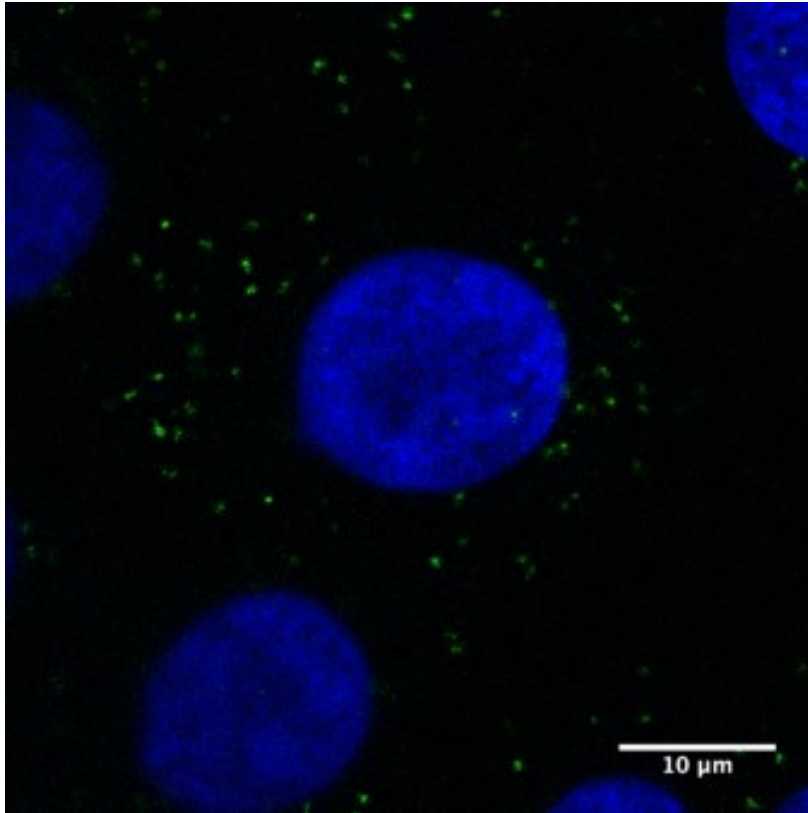
Figure 18. In situ detection of individual RNA molecules

The *in situ* RNA detection approach requires cDNA synthesis by a locked nucleic acid (LNA) primer, padlock probe hybridization and ligation onto the cDNA, and rolling circle amplification of the cDNA to detect the target RNA. The human $\boldsymbol{\beta}$-actin in HeLa cells was detected by Cy3-labeled detection probe (green).
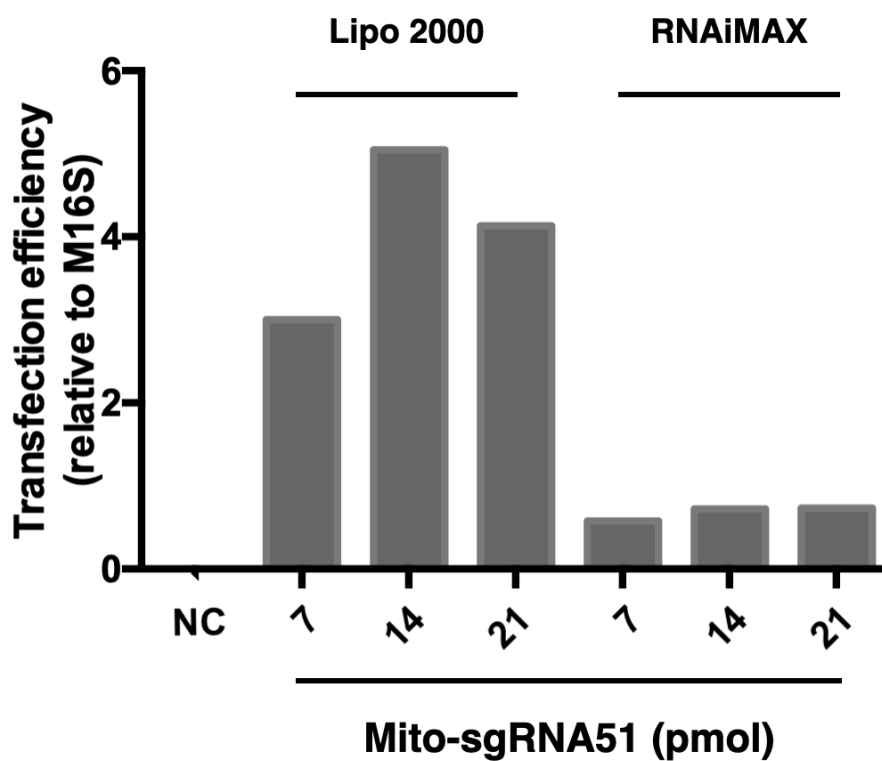
Figure 19. Mito-sgRNA51 transection efficiency optimization in 24-well plate

To optimize the transfection efficiency of mito-sgRNA51, we tested mito-sgRNA51

transfection by lipofectamine 2000 and RNAi MAX reagents. The cells were incubated

for nine hours after transfection and total RNA was extracted for RT-qPCR analysis of

the mito-sgRNA51 abundance relative to M16S. Compared to RNAi MAX transfection,

lipofectamine 2000 transfection could yield five-fold efficiency.
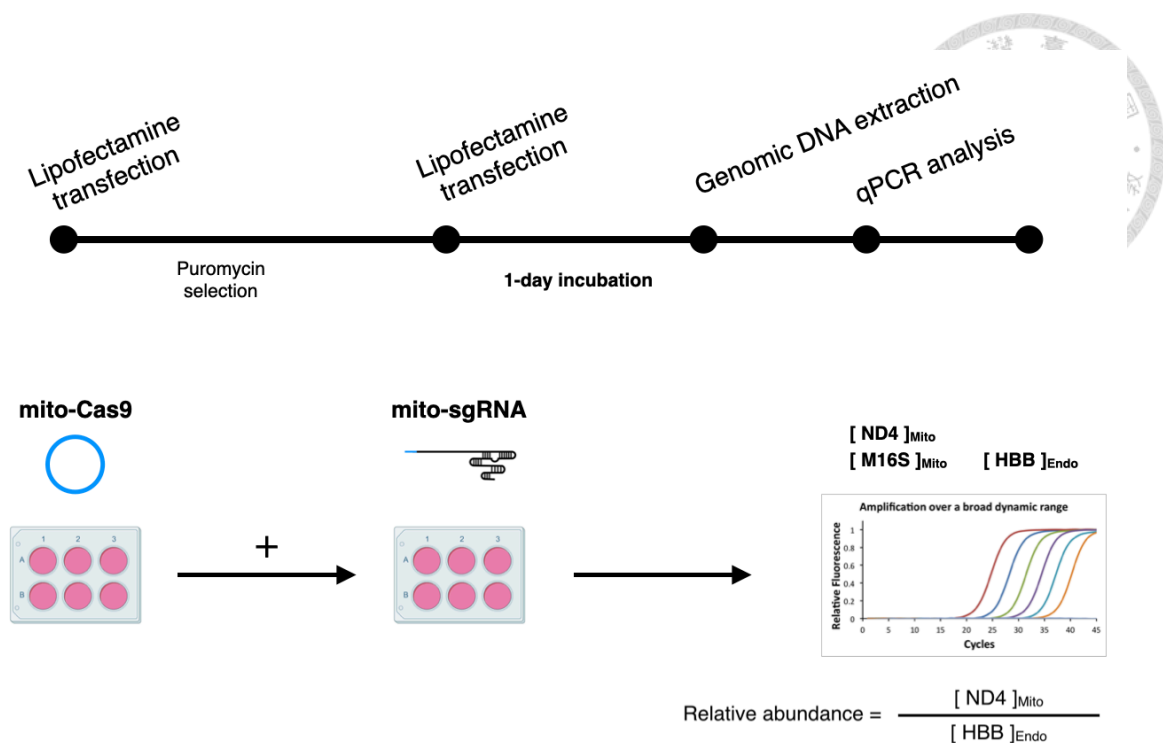
Figure 20. Schematic flow chart for mtDNA targeting by the mito-Cas9 system

To evaluate the robustness of the mito-Cas9 system for mtDNA targeting, we transfected mito-Cas9 plasmid (pSL241) into HeLa cells and performed puromycin selection for one day. Then, we delivered *in vitro* transcribed ND4-targeting mito-sgRNA into the cells. After one-day incubation, the cellular DNA was extracted and the mtDNA level were analyzed by calculating the ND4 abundance relative to HBB using the Ct value obtained from qPCR. Meanwhile, we also analyzed the M16S abundance relative to HBB to verify the mtDNA degradation caused after mito-Cas9 targeting.
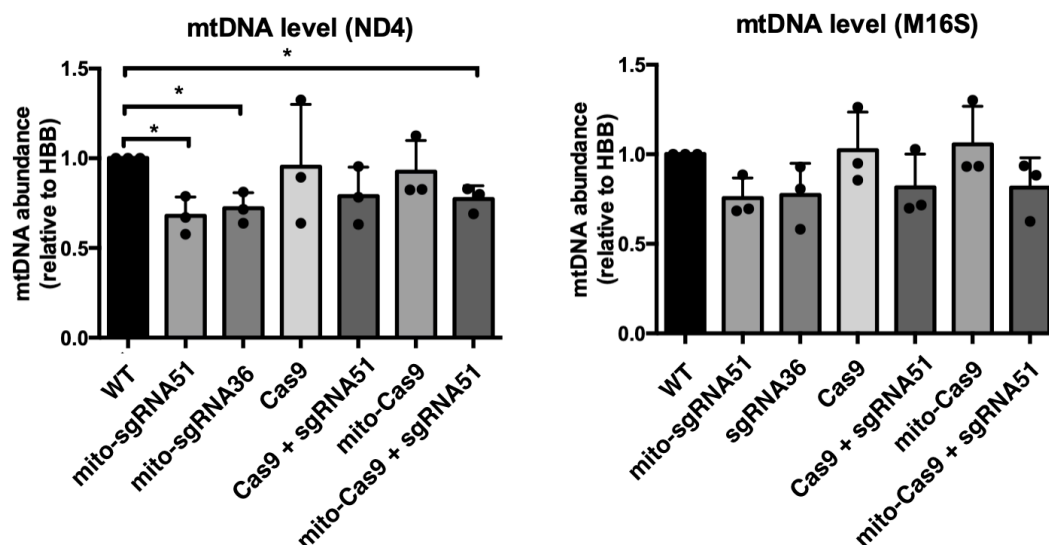
Figure 21. The mtDNA level in HeLa cells was interfered by mito-sgRNA delivery

The mito-sgRNA can cause interference with the mtDNA level in HeLa cells. After

delivering the mito-Cas9 system into the cells, it showed that the mtDNA level of ND4

was significantly decreased in the mito-sgRNA groups (32% reduction in mito-

sgRNA51 and 28% reduction in mito-sgRNA36). The mito-sgRNA interference is a

hurdle for the mtDNA targeting by mito-Cas9 system (n=3, t-test P<0.05).

59
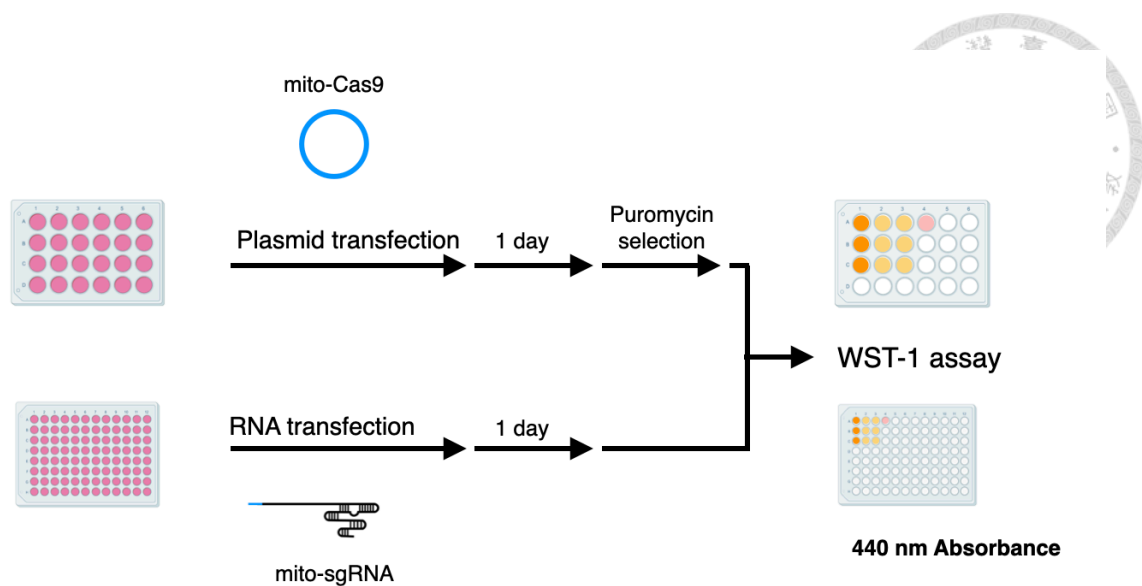
Figure 22. Schematic flow chart for cell viability assay of the mito-Cas9 system expression

To evaluate the cell viability affected by mito-Cas9 system expression, we transfected the mito-Cas9 plasmid (pSL241) and mito-sgRNAs into HeLa cells respectively. One day after RNA transfection and two days after plasmid transfection, the HeLa cells were treated with WST-1 reagent. Then, the relative cell viability was determined by comparing the 440nm wavelength absorbance of the sample medium to its respective control group.
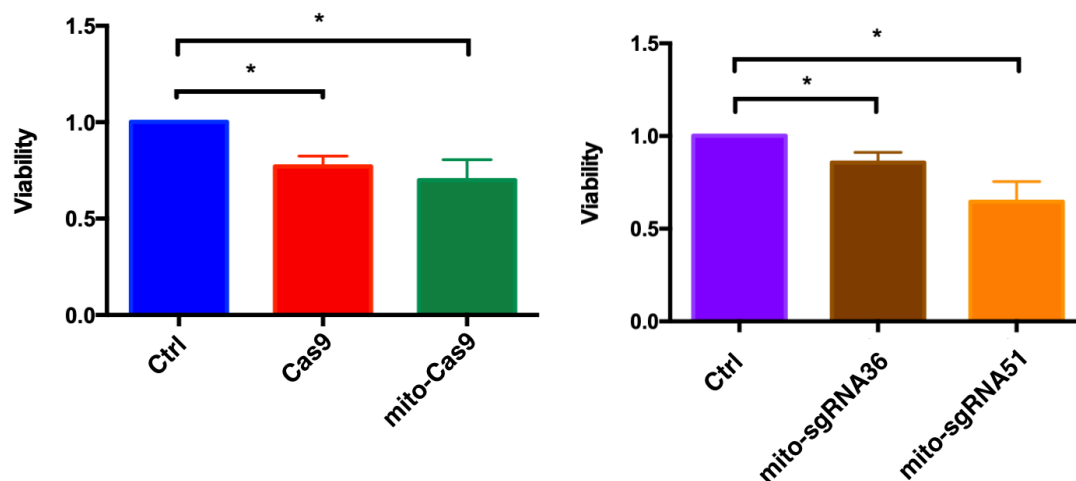
Figure 23. Decreased cell viability by mito-Cas9 system expression in HeLa cell line

Mito-Cas9 system expression can decrease the cell viability. After transfection of the mito-Cas9 system, the WST-1 assay showed that mito-Cas9 expression caused a decreased cell viability to 70% compared to control cells, which were puromycin resistant HeLa cells. The results also showed that Cas9 expression could lead the cell viability to 77% compared to control cells. As for mito-sgRNAs, mito-sgRNA36 led to an 85% viability, and mito-sgRNA51 caused a 64% viability compared to mock samples (n-3, t-test P<0.05).
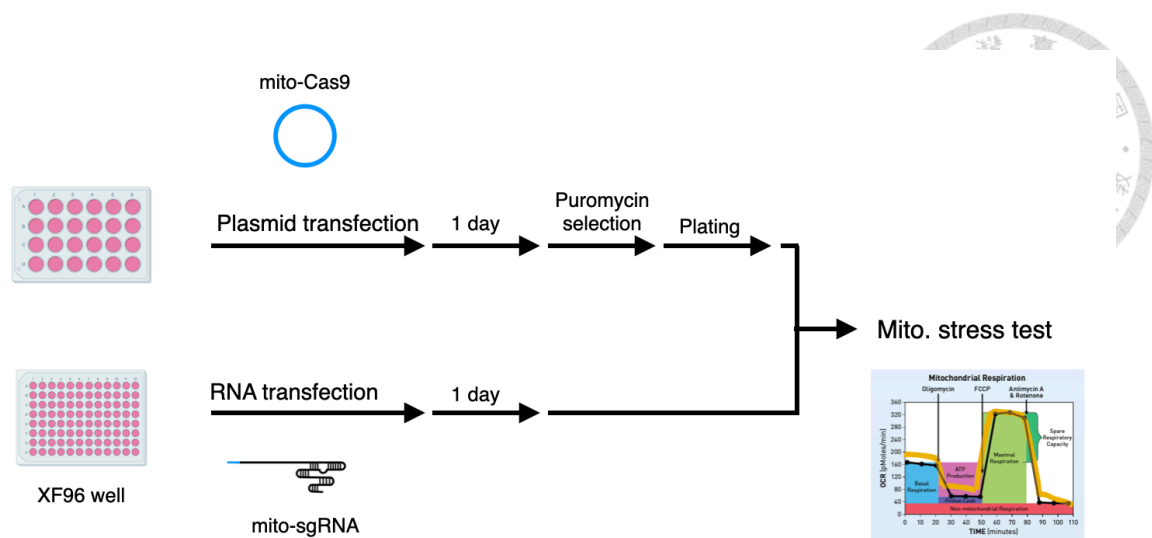
Figure 24. Schematic flow chart for Seahorse assay of the mito-Cas9 system expression

To evaluate the mitochondrial function affected by mito-Cas9 system expression, we transfected the mito-Cas9 plasmid (pSL241) and mito-sgRNAs into HeLa cells respectively. One day after RNA transfection and three days after plasmid transfection, the HeLa cells were treated with mitochondria stress test reagents, oligomycin, carbonyl cyanite-4 (trifluoromethoxyl) phenylhydrazone (FCCP), and Rotenone/Antimycin A (R/A) to obtain the oxygen consumption rate profile by the Seahorse XFe96 analyzer.
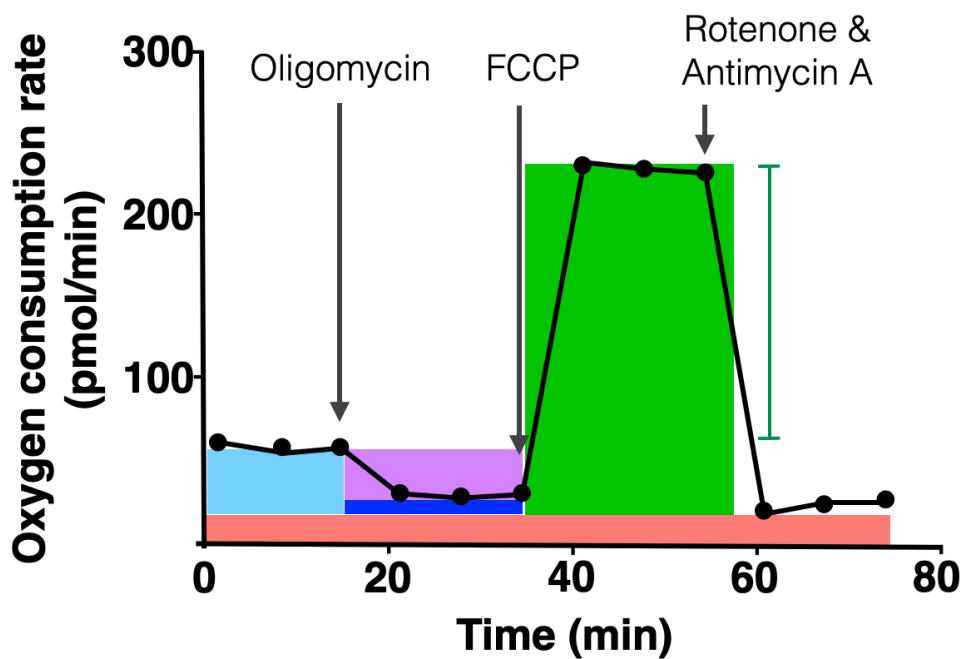
62

Figure 25. Seahorse XF cell mito stress test profile

The mito stress test measures the oxygen consumption rate of the cells during the injection of respiration moderators, oligomycin, carbonyl cyanite-4 (trifluoromethoxyl) phenylhydrazone (FCCP), and Rotenone/Antimycin A to obtain the parameters of the cell condition, including basal respiration (light blue), ATP production (purple), proton leak (dark blue), maximal respiration (light green), spare capacity (green bar), and non-mitochondrial respiration (carnation pink).

63
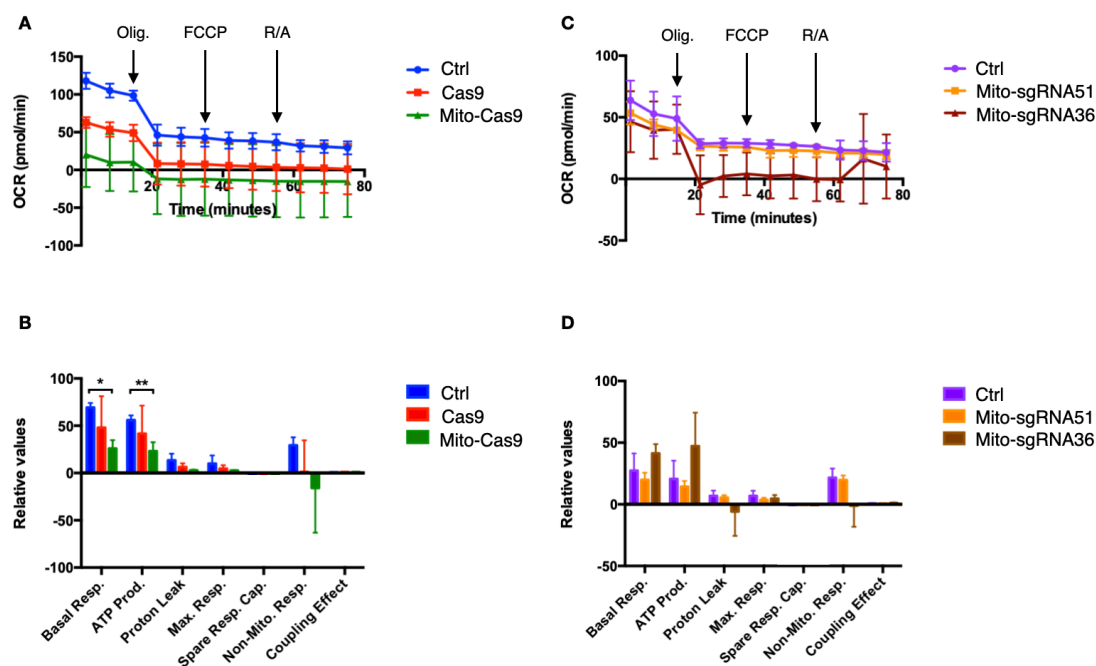
Figure 26. Mitochondrial respiration is impaired by mito-Cas9 expression in HeLa cells

Mito-Cas9 expression can cause a decreased mitochondrial respiration rate in HeLa cells. (A) Profile of Mito Stress Test data for Oxygen consumption rate (OCR) in HeLa cells with mito-Cas9 or Cas9 expression and control. Arrows indicate injections of specific stressors oligomycin (Olig.), carbonyl cyanite-4 (trifluoromethoxyl) phenylhydrazone (FCCP), and Rotenone/Antimycin A (R/A) (B) Relative values of parameters in HeLa cells with mito-Cas9 or Cas9 expression and control. The basal respiration and ATP production rate were significantly lower in mito-Cas9 expression HeLa cells compared to control. (C) Profile of Mito Stress Test data for OCR in HeLa cells with mito-sgRNA delivery and control. (D) Relative values of parameters in HeLa cells with mito-sgRNA delivery and control (n=3, t-test *P<0.05, **P<0.01).

Tables
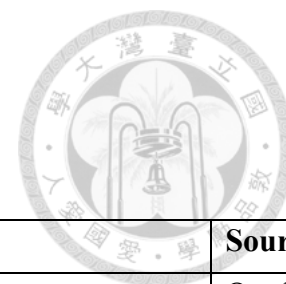
Table 1. Strains, plasmids, and primers used in this study

Strain	Characteristics	Source
209	pSL127	Our lab
212	pSL127B	Our lab
216	pSL127C	Our lab
218	pSL127D	Our lab
213	pSL127E	Our lab
215	pSL127F	Our lab
214	pSL127G	Our lab
418	pSL292	Our lab
429	pSL293	Our lab
436	pSL294	This work
433	pSL295	This work
447	pSL240	This work
450	pSL241	This work
467	pSL331	This work
491	pSL284	This work
496	pSL288	This work
497	pSL311	This work
498	pSL312	This work
505	pSL313	This work
512	pSL314	This work
513	pSL317	This work
Plasmid	**Characteristics**	**Source**
pCMVΔR8.91	CMV-Gag-Pol-Tat-Rev-PolyA	Our lab
pMD.G	hCMV-beta globin intron-VSV.G-beta globin polyA	Our lab
Mito-EGFP	2xCOX8A MTS-EGFP-Kan^R	Our lab
pSL127	BamHI-Cas9-3xFLAG-NheI	Our lab
pSL127B	2xCOX8A MTS-Cas9-3xFLAG-NheI	Our lab
pSL127C	COX4P MTS-Cas9-3xFLAG-NheI	Our lab
pSL127D	ACACB MTS-Cas9-3xFLAG-NheI	Our lab
pSL127E	GLDC MTS-Cas9-3xFLAG-NheI	Our lab

pSL127F	POLG MTS-Cas9-3xFLAG-NheI	Our lab
pSL127G	MTHFD1L MTS-Cas9-3xFLAG-NheI	Our lab
pSL292	3xFLAG-Cas9-turboGFP (TetOn)	Our lab
pSL293	MTS-3xFLAG-Cas9-turboGFP (TetOn)	Our lab
pSL294	Kozak-3xFLAG-Cas9-turboGFP	This work
pSL295	Kozak-MTS-3xFLAG-Cas9-turboGFP	This work
pSL240	3xFLAG-Cas9-P2A-PAC (hPGK promoter)	This work
pSL241	MTS-3xFLAG-Cas9-P2A-PAC (hPGK promoter)	This work
pSL331	hPGK-MTS-Cas9-3xFLAG	This work
pSL284	hPGK-PAC	This work
pSL288	sgRNA scaffold-hPGK-PAC	This work
pSL311	sgRNA51-Cas9-FLAG	This work
pSL312	sgRNA51-MTS-Cas9-FLAG	This work
pSL313	sgRNA scaffold-hPGK-FLAG-Cas9-P2A-PAC	This work
pSL314	sgRNA51-Kozak-FLAG-Cas9-turboGFP	This work
pSL317	sgRNA51-Kozak-MTS-FLAG-Cas9-turboGFP	This work
pSL331	hPGK-MTS-Cas9-3xFLAG	This work

Primer	Sequence (5'-3')	Purpose
P-BE1	A+TC+AT+CC+AT+GG+TG+AGCTGGCGGCGG (+ symbol denotes the locked nucleic acid base)	*β*-actin *In situ* hybridization
P-TERT	A+GG+AC+AC+CT+GG+CG+GAAGGAGGGGGCGGCGG	TERT *In situ* hybridization
PLP-BE1	AGCCTCGCCTTTGCCTTCCTTTTACGACCTCAATGCTGCTGCTGTACTA CTCTTCGCCCCGCGAGCACAG	*β*-actin *In situ* hybridization
PLP-TERT	GGTGTGCGTGCCCTGGGACGACTTTCTATGATTACTGACCTACCTCAAT GCACATGTTTGGCTCCTCTTCGCGCTGGTGGCCCAGTGCCT	TERT *In situ* hybridization
DP-1	Cy3-CCTCAATGCTGCTGCTGTACTAC	*In situ* hybridization
DP-2	Cy5-CCTCAATGCACATGTTTGGCTCC	*In situ* hybridization
SL752	GTAGCGCTAGGCATTCCAAGGCACAGCAGTGGTG	pSL240/241
SL753	CCTTGGAATGCCTAGCGCTACCGGTTGCAGGAATTC	pSL240/241

66

SL754	CATGGTGGCAAGCTCCGGTGGATCCCCCTG	pSL240/241
SL755	CACCGGAGCTTGCCACCATGGGATCCGGAGGTG	pSL240
SL756	CTGCCGTCGCCTCCCAGCTGAGACAGGTC	pSL240/241
SL757	CAGCTGGGAGGCGACGGCAGCGGCGCTACAAATTTCAG	pSL240/241
SL758	GTACTCGGTCATGCCGGAGCCACCAGGTCCAG	pSL240/241
SL759	GCTCCGGCATGACCGAGTACAAGCCCACGGTG	pSL240/241
SL760	CACCGGAGCTTGCCACCATGGGCACTCGCTTGC	pSL241
MF16	CGAGCTACCTAAGAACAGCTAAA	M16S qPCR
MF17	TCTTGGACAACCAGCTATCAC	M16S qPCR
Max 52	CTAGAGGTACCGGGTTGCGCCTTTTCCAAGGC	pSL331
Max 55	GCGCAACCCGGTACCTCTAGAGCCATTTGTCTG	pSL331
Max 58	CTCCCCAGGGTTGGATGGGCACTCGCTTGC	pSL331
Max 59	GTGCCCATCCAACCCTGGGGAGAGAGGTCGGTG	pSL331
Max 60	TCGGGAAGGTTCCTTGCGGTTCGC	PCR check
Max 61	TGAGGAAGAGTTCTTGCAGCTCGGTGACC	PCR check
Max 62	CAGTCATTCTCATAATCGCCCACGGA	ND4 qPCR
Max 63	GGTAAGGCGAGGTTAGCGAGGC	ND4 qPCR
Max 64	CAATCAGCCACATAGCCCTCGTAGTAAC	ND4 qPCR
Max 65	AAGCTATTAGTGGGAGTAGAGTTTGAAGC	ND4 qPCR
Max 66	ACCGAGTACAAGCCCACGGTG	PAC vector
Max 67	GCCCATGGTGGCAAGCTCCG	PAC vector
Max 68	ACTCCTAAGCCAGTGCCAGAAG	HBB qPCR
Max 69	TCTGCCCTGACTTTTATGCCCA	HBB qPCR
Max 70	CTAGAGGTACCGGGTTGCGCCTTTTCCAAGGCAG	pSL313
Max 71	GGAATTCTTATCATCAGGCACCGGGCTTGCG	pSL313
Max 72	CGGTGCCTGATGATAAGAATTCCTAGAGCTCGCTGATC	pSL288/313
Max 73	GGCGCAACCCGGTACCTCTAGAGCCATTTGTCTGCAG	pSL288/313
Max 74	CGGTGCCTGATGATAAGAATTCCTAGAGCTCGCTGATC AGCCTCG	pSL288/313
Max 75	GGCGCAACCCGGTACCTCTAGAGCCATTTGTCTGCAG AATTGGC	pSL288/313
Max 76	CACCGCACTCACAGTCGCATCATAATCCTCTCTCA	pSL311/312/ 314/317

Max 77	AAACTGAGAGAGGATTATGATGCGACTGTGAGTGC	pSL311/312/ 314/317

Table 2. Humanized SpCas9 sequence and mitochondria-targeting sequences

Gene	Sequence (5'-3')
Human codon optimized S. pyogenes Cas9	GACAAGAAGTACAGCATCGGCCTGGACATCGGC ACCAACTCTGTGGGCTGGGCCGTGATCACCGAC GAGTACAAGGTGCCCAGCAAGAAATTCAAGGTG CTGGGCAACACCGACCGGCACAGCATCAAGAAG AACCTGATCGGAGCCCTGCTGTTCGACAGCGGC GAAACAGCCGAGGCCACCCGGCTGAAGAGAACC CGCCAGAAGAAGATACACCAGACGGAAGAACC GGATCTGCTATCTGCAAGAGATCTTCAGCAACG AGATGGCCAAGGTGGACGACAGCTTCTTCCACA GACTGGAAGAGTCCTTCCTGGTGGAAGAGGATA AGAAGCACGAGCGGCACCCCATCTTCGGCAACA TCGTGGACGAGGTGGCCTACCACGAGAAGTACC CCACCATCTACCACCTGAGAAAGAAACTGGTGG ACAGCACCGACAAGGCCGACCTGCGGCTGATCT ATCTGGCCCTGGCCCACATGATCAAGTTCCGGG GCCACTTCCTGATCGAGGGCGACCTGAACCCCG ACAACAGCGACGTGGACAAGCTGTTCATCCAGC TGGTGCAGACCTACAACCAGCTGTTCGAGGAAA ACCCCATCAACGCCAGCGGCGTGGACGCCAAGG CCATCCTGTCTGCCAGACTGAGCAAGAGCAGAC GGCTGGAAAATCTGATCGCCCAGCTGCCCGGCG AGAAGAAGAATGGCCTGTTCGGAAACCTGATTG CCCTGAGCCTGGGCCTGACCCCCAACTTCAAGA GCAACTTCGACCTGGCCGAGGATGCCAAACTGC AGCTGAGCAAGGACACCTACGACGACGACCTGG ACAACCTGCTGGCCCAGATCGGCGACCAGTACG CCGACCTGTTTCTGGCCGCCAAGAACCTGTCCGA CGCCATCCTGCTGAGCGACATCCTGAGAGTGAA CACCGAGATCACCAAGGCCCCCCTGAGCGCCTC TATGATCAAGAGATACGACGAGCACCACCAGGA CCTGACCCTGCTGAAAGCTCTCGTGCGGCAGCA GCTGCCTGAGAAGTACAAAGAGATTTTCTTCGA CCAGAGCAAGAACGGCTACGCCGGCTACATTGA CGGCGGAGCCAGCCAGGAAGAGTTCTACAAGTT CATCAAGCCCATCCTGGAAAAGATGGACGGCAC CGAGGAACTGCTCGTGAAGCTGAACAGAGAGGA CCTGCTGCGGAAGCAGCGGACCTTCGACAACGG CAGCATCCCCCACCAGATCCACCTGGGAGAGCT GCACGCCATTCTGCGGCGGCAGGAAGATTTTTA CCCATTCCTGAAGGACAACCGGGAAAAGATCGA

	GAAGATCCTGACCTTCCGCATCCCCTACTACGTG
	GGCCCTCTGGCCAGGGGAAACAGCAGATTCGCC
	TGGATGACCAGAAAGAGCGAGGAAACCATCACC
	CCCTGGAACTTCGAGGAAGTGGTGGACAAGGGC
	GCTTCCGCCCAGAGCTTCATCGAGCGGATGACC
	AACTTCGATAAGAACCTGCCCAACGAGAAGGTG
	CTGCCCAAGCACAGCCTGCTGTACGAGTACTTC
	ACCGTGTATAACGAGCTGACCAAAGTGAAATAC
	GTGACCGAGGGAATGAGAAAGCCCGCCTTCCTG
	AGCGGCGAGCAGAAAAAGGCCATCGTGGACCTG
	CTGTTCAAGACCAACCGGAAAGTGACCGTGAAG
	CAGCTGAAAGAGGACTACTTCAAGAAAATCGAG
	TGCTTCGACTCCGTGGAAATCTCCGGCGTGGAA
	GATCGGTTCAACGCCTCCCTGGGCACATACCAC
	GATCTGCTGAAAATTATCAAGGACAAGGACTTC
	CTGGACAATGAGGAAAACGAGGACATTCTGGAA
	GATATCGTGCTGACCCTGACACTGTTTGAGGAC
	AGAGAGATGATCGAGGAACGGCTGAAAACCTAT
	GCCCACCTGTTCGACGACAAAGTGATGAAGCAG
	CTGAAGCGGCGGAGATACACCGGCTGGGGCAGG
	CTGAGCCGGAAGCTGATCAACGGCATCCGGGAC
	AAGCAGTCCGGCAAGACAATCCTGGATTTCCTG
	AAGTCCGACGGCTTCGCCAACAGAAACTTCATG
	CAGCTGATCCACGACGACAGCCTGACCTTTAAA
	GAGGACATCCAGAAAGCCCAGGTGTCCGGCCAG
	GGCGATAGCCTGCACGAGCACATTGCCAATCTG
	GCCGGCAGCCCCGCCATTAAGAAGGGCATCCTG
	CAGACAGTGAAGGTGGTGGACGAGCTCGTGAAA
	GTGATGGGCCGGCACAAGCCCGAGAACATCGTG
	ATCGAAATGGCCAGAGAGAACCAGACCACCCAG
	AAGGGACAGAAGAACAGCCGCGAGAGAATGAA
	GCGGATCGAAGAGGGCATCAAAGAGCTGGGCA
	GCCAGATCCTGAAAGAACACCCCGTGGAAAACA
	CCCAGCTGCAGAACGAGAAGCTGTACCTGTACT
	ACCTGCAGAATGGGCGGGATATGTACGTGGACC
	AGGAACTGGACATCAACCGGCTGTCCGACTACG
	ATGTGGACCATATCGTGCCTCAGAGCTTTCTGAA
	GGACGACTCCATCGACAACAAGGTGCTGACCAG
	AAGCGACAAGAACCGGGGCAAGAGCGACAACG
	TGCCCTCCGAAGAGGTCGTGAAGAAGATGAAGA
	ACTACTGGCGGCAGCTGCTGAACGCCAAGCTGA
	TTACCCAGAGAAAGTTCGACAATCTGACCAAGG
	CCGAGAGAGGCGGCCTGAGCGAACTGGATAAG
	GCCGGCTTCATCAAGAGACAGCTGGTGGAAACC
	CGGCAGATCACAAAGCACGTGGCACAGATCCTG
	GACTCCCGGATGAACACTAAGTACGACGAGAAT
	GACAAGCTGATCCGGGAAGTGAAAGTGATCACC
	CTGAAGTCCAAGCTGGTGTCCGATTTCCGGAAG
	GATTTCCAGTTTTACAAAGTGCGCGAGATCAAC
	AACTACCACCACGCCCACGACGCCTACCTGAAC

GCCGTCGTGGGAACCGCCCTGATCAAAAAGTAC
CCTAAGCTGGAAAGCGAGTTCGTGTACGGCGAC
TACAAGGTGTACGACGTGCGGAAGATGATCGCC
AAGAGCGAGCAGGAAATCGGCAAGGCTACCGC
CAAGTACTTCTTCTACAGCAACATCATGAACTTT
TTCAAGACCGAGATTACCCTGGCCAACGGCGAG
ATCCGGAAGCGGCCTCTGATCGAGACAAACGGC
GAAACCGGGGAGATCGTGTGGGATAAGGGCCG
GGATTTTGCCACCGTGCGGAAAGTGCTGAGCAT
GCCCCAAGTGAATATCGTGAAAAAGACCGAGGT
GCAGACAGGCGGCTTCAGCAAAGAGTCTATCCT
GCCCAAGAGGAACAGCGATAAGCTGATCGCCAG
AAAGAAGGACTGGGACCCTAAGAAGTACGGCG
GCTTCGACAGCCCCACCGTGGCCTATTCTGTGCT
GGTGGTGGCCAAAGTGGAAAAGGGCAAGTCCA
AGAAACTGAAGAGTGTGAAAGAGCTGCTGGGG
ATCACCATCATGGAAAGAAGCAGCTTCGAGAAG
AATCCCATCGACTTTCTGGAAGCCAAGGGCTAC
AAAGAAGTGAAAAAGGACCTGATCATCAAGCTG
CCTAAGTACTCCCTGTTCGAGCTGGAAAACGGC
CGGAAGAGAATGCTGGCCTCTGCCGGCGAACTG
CAGAAGGGAAACGAACTGGCCCTGCCCTCCAAA
TATGTGAACTTCCTGTACCTGGCCAGCCACTATG
AGAAGCTGAAGGGCTCCCCCGAGGATAATGAGC
AGAAACAGCTGTTTGTGGAACAGCACAAGCACT
ACCTGGACGAGATCATCGAGCAGATCAGCGAGT
TCTCCAAGAGAGTGATCCTGGCCGACGCTAATC
TGGACAAAGTGCTGTCCGCCTACAACAAGCACC
GGGATAAGCCCATCAGAGAGCAGGCCGAGAAT
ATCATCCACCTGTTTACCCTGACCAATCTGGGAG
CCCCTGCCGCCTTCAAGTACTTTGACACCACCAT
CGACCGGAAGAGGTACACCAGCACCAAAGAGG
TGCTGGACGCCACCCTGATCCACCAGAGCATCA
CCGGCCTGTACGAGACACGGATCGACCTGTCTC
AGCTGGGAGGCGAC

Translation:
DKKYSIGLDIGTNSVGWAVITDEYKVPSKKFKVLG
NTDRHSIKKNLIGALLFDSGETAEATRLKRTARRR
YTRRKNRICYLQEIFSNEMAKVDDSFFHRLEESFLV
EEDKKHERHPIFGNIVDEVAYHEKYPTIYHLRKKL
VDSTDKADLRLIYLALAHMIKFRGHFLIEGDLNPD
NSDVDKLFIQLVQTYNQLFEENPINASGVDAKAILS
ARLSKSRRLENLIAQLPGEKKNGLFGNLIALSLGLT
PNFKSNFDLAEDAKLQLSKDTYDDDLDNLLAQIG
DQYADLFLAAKNLSDAILLSDILRVNTEITKAPLSA
SMIKRYDEHHQDLTLLKALVRQQLPEKYKEIFFDQ
SKNGYAGYIDGGASQEEFYKFIKPILEKMDGTEEL
LVKLNREDLLRKQRTFDNGSIPHQIHLGELHAILRR
QEDFYPFLKDNREKIEKILTFRIPYYVGPLARGNSR

	FAWMTRKSEETITPWNFEEVVDKGASAQSFIERMT NFDKNLPNEKVLPKHSLLYEYFTVYNELTKVKYV TEGMRKPAFLSGEQKKAIVDLLFKTNRKVTVKQL KEDYFKKIECFDSVEISGVEDRFNASLGTYHDLLKI IKDKDFLDNEENEDILEDIVLTLTLFEDREMIEERL KTYAHLFDDKVMKQLKRRRYTGWGRLSRKLINGI RDKQSGKTILDFLKSDGFANRNFMQLIHDDSLTFK EDIQKAQVSGQGDSLHEHIANLAGSPAIKKGILQT VKVVDELVKVMGRHKPENIVIEMARENQTTQKGQ KNSRERMKRIEEGIKELGSQILKEHPVENTQLQNE KLYLYYLQNGRDMYVDQELDINRLSDYDVDHIVP QSFLKDDSIDNKVLTRSDKNRGKSDNVPSEEVVKK MKNYWRQLLNAKLITQRKFDNLTKAERGGLSELD KAGFIKRQLVETRQITKHVAQILDSRMNTKYDEND KLIREVKVITLKSKLVSDFRKDFQFYKVREINNYH HAHDAYLNAVVGTALIKKYPKLESEFVYGDYKVY DVRKMIAKSEQEIGKATAKYFFYSNIMNFFKTEITL ANGEIRKRPLIETNGETGEIVWDKGRDFATVRKVL SMPQVNIVKKTEVQTGGFSKESILPKRNSDKLIARK KDWDPKKYGGFDSPTVAYSVLVVAKVEKGKSKK LKSVKELLGITIMERSSFEKNPIDFLEAKGYKEVKK DLIIKLPKYSLFELENGRKRMLASAGELQKGNELA LPSKYVNFLYLASHYEKLKGSPEDNEQKQLFVEQ HKHYLDEIIEQISEFSKRVILADANLDKVLSAYNKH RDKPIREQAENIIHLFTLTNLGAPAAFKYFDTTIDR KRYTSTKEVLDATLIHQSITGLYETRIDLSQLGGD
2x COX8A MTS	ATGAGTGTGCTGACGCCACTGCTGCTGAGAGGA CTGACAGGCAGTGCTCGGAGACTCCCAGTACCT AGAGCAAAAATTCATTCTCTTGGAGATCTTTCCG TATTGACTCCTTTGTTGTTGAGAGGCTTGACAGG ATCGGCTAGACGGCTCCCAGTGCCGCGCGCCAA GATCCACTCGCTGGGGGAC Translation: MSVLTPLLLRGLTGSARRLPVPRAKIHSLGDLSVLT PLLLRGLTGSARRLPVPRAKIHSLGD
S. cerevisiae COX4P MTS	ATGAGTGTGCTGACGCCACTGCTGCTGAGAGGA CTGACAGGCAGTGCTCGGAGACTCCCAGTACCT AGAGCAAAAATTCATTCTCTTGGAGATCTTTCCG TATTGACTCCTTTGTTGTTGAGAGGCTTGACAGG ATCGGCTAGACGGCTCCCAGTGCCGCGCGCCAA GATCCACTCGCTGGGGGAC Translation: MSVLTPLLLRGLTGSARRLPVPRAKIHSLGDLSVLT PLLLRGLTGSARRLPVPRAKIHSLGD
ACACB MTS	ATGGTTCTGCTGCTGTGCTTGAGCTGCCTTATTT TCAGTTGCCTTACATTTTCTTGGCTCAAAATTTG GGGCAAGATGACTGATTCCAAGCCTATTACCAA AAGCAAGTCAGAGGCGAAC

	Translation: MVLLLCLSCLIFSCLTFSWLKIWGKMTDSKPITKSK SEAN
GLDC MTS	ATGCAGTCTTGTGCTAGAGCCTGGGGGCTGAGA TTGGGGAGGGGTGTCGGGGGGGGCAGAAGGTTG GCCGGTGGGAGTGGACCATGTTGGGCTCCTAGA AGTCGC Translation: MQSCARAWGLRLGRGVGGGRRLAGGSGPCWAPR SR
POLG MTS	ATGTCTCGGCTGCTTTGGAGAAAGGTCGCGGGG GCGACAGTCGGTCCTGGTCCAGTCCCTGCGCCC GGTCGCTGGGTCTCATCCAGTGTTCCTGCTTCAG ATCCATCTGATGGA Translation: MSRLLWRKVAGATVGPGPVPAPGRWVSSSVPASD PSDG
MTHFD1L MTS	ATGGGCACTCGCTTGCCTCTCGTGTTGCGACAGT TGAGGCGGCCGCCGCAACCTCCCGGTCCCCCCC GAAGGTTGCGAGTTCCATGCCGAGCA Translation: MGTRLPLVLRQLRRPPQPPGPPRRLRVPCRA

Table 3. T7 in vitro transcribed RNA (IVT RNA) used in this study

IVT RNA	Sequence (5'-3')	Target gene
sgRNA36	<u>GCATCATAATCCTCTCTCAGTTTAAGAGC</u> TATGCTGGAAACAGCATAGCAAGTTTAA ATAAGGCTAGTCCGTTATCAACTTGAAA AAGTGGCACCGAGTCGGTGC	19nt ND4 target 6
sgRNA51	<u>GCACTCACAGTCGCATCATAATCCTCTCT CA</u>GTTTAAGAGCTATGCTGGAAACAGCA TAGCAAGTTTAAATAAGGCTAGTCCGTTA TCAACTTGAAAAAGTGGCACCGAGTCGG TGC	30 nt ND4 target 6

*Underlined letters: sgRNA target sequence.
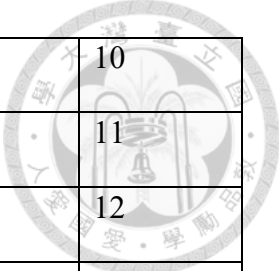
Table 4. PCR condition of DNA template synthesis for IVT RNA

IVT RNA	Reaction set up		Thermal cycler set up
sgRNA36	Molecular water	33ul	**Applied Biosystems**
	5x KAPA HiFi fidelity buffer	12ul	**SimpliAmp**
	dimethyl sulfoxide (DMSO)	6ul	

	10 uM T25G/SLKS2	2ul	98°C, 2 minutes
	1 uM SL467/SL297	4ul	98°C, 10 seconds \
	KAPA dNTP mix	1.8ul	62°C, 10 seconds | 40 cycles
	KAPA HiFi DNA polymerase	1.2ul	72°C, 10 seconds /
		60ul	72°C, 2 minutes
			12°C, 5 minutes
sgRNA51	Molecular water	33ul	**Eppendorf 6325**
	5x KAPA HiFi fidelity buffer	12ul	**Mastercycler Pro S**
	dimethyl sulfoxide (DMSO)	6ul	
	1 uM SL613/SLKS2	3.6ul	98°C, 2 minutes
	1 ng/ul pSL146	2.4ul	98°C, 10 seconds \
	KAPA dNTP mix	1.8ul	61°C, 10 seconds | 40 cycles
	KAPA HiFi DNA polymerase	1.2ul	72°C, 15 seconds /
		60ul	72°C, 2 minutes
			12°C, 5 minutes

Table 5. Plasmid construction in this study

Plasmid	Primer set	Template	Amplicon
pSL127	SL434, SL439	pAW006	1
	SL435, SL436	pAW006	2
	SL437, SL438	pAW006	3
pSL127B	SL448, SL449	pSL127	4
	SL456, SL457	SL533	5
pSL127C	SL448, SL449	pSL127	4
	SL460, SL461	SL533	6
pSL127D	SL448, SL449	pSL127	4
	SL450, SL451	SL533	7
pSL127E	SL448, SL449	pSL127	4
	SL454, SL455	SL533	8
pSL127F	SL448, SL449	pSL127	4
	SL452, SL453	SL533	9
pSL127G	SL448, SL449	pSL127	4

	SL458, SL459	SL533	10
pSL294	SL726, SL704	pSL131	11
	SL705, SL719	pMaxGFP	12
	SL717, SL725	pX330	13
pSL295	SL720, SL719	pSL293	14
	SL717, SL716	pX330	15
pSL292	SL709, SL704	pSL131	16
	SL705, SL707	pMaxGFP	17
	SL706, SL703	pSL170	18
pSL293	SL709, SL707	pSL292	19
	SL706, SL708	pSL171	20
pSL240	SL759, SL752	pSL141	21
	SL753, SL754	pSL141	22
	SL755, SL756	pSL294	23
	SL757, SL758	pSL486	24
pSL241	SL759, SL752	pSL141	21
	SL753, SL754	pSL141	22
	SL760, SL756	pSL295	25
	SL757, SL758	pSL486	24

Reference

1   McBride, H. M., Neuspiel, M. & Wasiak, S. Mitochondria: more than just a powerhouse. *Curr Biol* **16**, R551-560, doi:10.1016/j.cub.2006.06.054 (2006).

2   Wallace, D. C. Mitochondrial genetic medicine. *Nature genetics* **50**, 1642-1649, doi:10.1038/s41588-018-0264-z (2018).

3   Yu-Wai-Man, P., Turnbull, D. M. & Chinnery, P. F. Leber hereditary optic neuropathy. *Journal of medical genetics* **39**, 162-169, doi:10.1136/jmg.39.3.162 (2002).

4   Rahman, S. *et al.* Leigh syndrome: clinical features and biochemical and DNA abnormalities. *Annals of neurology* **39**, 343-351, doi:10.1002/ana.410390311 (1996).

5   Lake, N. J., Compton, A. G., Rahman, S. & Thorburn, D. R. Leigh syndrome: One disorder, more than 75 monogenic causes. *Annals of neurology* **79**, 190-203, doi:10.1002/ana.24551 (2016).

6   Degoul, F. *et al.* Deletions of mitochondrial DNA in Kearns-Sayre syndrome and ocular myopathies: Genetic, biochemical and morphological studies. *Journal of the Neurological Sciences* **101**, 168-177, doi:10.1016/0022-510X(91)90042-6 (1991).

7   Shoffner, J. M. *et al.* Myoclonic epilepsy and ragged-red fiber disease (MERRF) is associated with a mitochondrial DNA tRNALys mutation. *Cell* **61**, 931-937, doi:https://doi.org/10.1016/0092-8674(90)90059-N (1990).

8   Tuppen, H. A., Blakely, E. L., Turnbull, D. M. & Taylor, R. W. Mitochondrial DNA mutations and human disease. *Biochimica et biophysica acta* **1797**, 113-128, doi:10.1016/j.bbabio.2009.09.005 (2010).

9   Bacman, S. R., Williams, S. L., Duan, D. & Moraes, C. T. Manipulation of mtDNA heteroplasmy in all striated muscles of newborn mice by AAV9-mediated delivery of a mitochondria-targeted restriction endonuclease. *Gene therapy* **19**, 1101-1106, doi:10.1038/gt.2011.196 (2012).

10   Jenuth, J. P., Peterson, A. C. & Shoubridge, E. A. Tissue-specific selection for different mtDNA genotypes in heteroplasmic mice. *Nature genetics* **16**, 93-95, doi:10.1038/ng0597-93 (1997).

11   Van Houten, B., Hunter, S. E. & Meyer, J. N. Mitochondrial DNA damage induced autophagy, cell death, and disease. *Frontiers in bioscience (Landmark edition)* **21**, 42-54, doi:10.2741/4375 (2016).

12   Alexeyev, M. F. *et al.* Selective elimination of mutant mitochondrial genomes as therapeutic strategy for the treatment of NARP and MILS syndromes. *Gene therapy* **15**, 516-523, doi:10.1038/sj.gt.2008.11 (2008).

13   Tanaka, M. *et al.* Gene therapy for mitochondrial disease by delivering restriction endonuclease SmaI into mitochondria. *Journal of biomedical science* **9**, 534-541, doi:10.1159/000064726 (2002).

14   Bayona-Bafaluy, M. P., Blits, B., Battersby, B. J., Shoubridge, E. A. & Moraes, C. T. Rapid directional shift of mitochondrial DNA heteroplasmy in animal tissues by a mitochondrially targeted restriction endonuclease. *Proceedings of the National Academy of Sciences of the United States of America* **102**, 14392-14397, doi:10.1073/pnas.0502896102 (2005).

15   Minczuk, M., Papworth, M. A., Miller, J. C., Murphy, M. P. & Klug, A. Development of a single-chain, quasi-dimeric zinc-finger nuclease for the selective degradation of mutated human mitochondrial DNA. *Nucleic acids research* **36**, 3926-3938, doi:10.1093/nar/gkn313 (2008).

16   Reddy, P. *et al.* Selective Elimination of Mitochondrial Mutations in the Germline by Genome Editing. *Cell* **161**, 459-469, doi:10.1016/j.cell.2015.03.051 (2015).

17   Bacman, S. R., Williams, S. L., Pinto, M., Peralta, S. & Moraes, C. T. Specific elimination of mutant mitochondrial genomes in patient-derived cells by mitoTALENs. *Nature medicine* **19**, 1111-1113, doi:10.1038/nm.3261 (2013).

18   Hashimoto, M. *et al.* MitoTALEN: A General Approach to Reduce Mutant mtDNA Loads and Restore Oxidative Phosphorylation Function in Mitochondrial Diseases.

Molecular therapy : the journal of the American Society of Gene Therapy **23**, 1592-1599, doi:10.1038/mt.2015.126 (2015).

19   Jinek, M., Chylinski, K., Fonfara, I., Hauer, M., Doudna, J. A. & Charpentier, E. A programmable dual-RNA guided DNA endonuclease in adaptive bacterial immunity. *Science* **337**, 816-821 (2012).

20   Lakshmipathy, U. & Campbell, C. Double strand break rejoining by mammalian mitochondrial extracts. *Nucleic acids research* **27**, 1198-1204, doi:10.1093/nar/27.4.1198 (1999).

21   Bacman, S. R., Williams, S. L. & Moraes, C. T. Intra- and inter-molecular recombination of mitochondrial DNA after in vivo induction of multiple double-strand breaks. *Nucleic acids research* **37**, 4218-4226, doi:10.1093/nar/gkp348 (2009).

22   Wisnovsky, S., Jean, S. R., Liyanage, S., Schimmer, A. & Kelley, S. O. Mitochondrial DNA repair and replication proteins revealed by targeted chemical probes. *Nature Chemical Biology* **12**, 567-573, doi:10.1038/nchembio.2102 (2016).

23   Weber-Lotfi, F. *et al.* Nucleic acid import into mitochondria: New insights into the translocation pathways. *Biochimica et Biophysica Acta (BBA) - Molecular Cell Research* **1853**, 3165-3181, doi:https://doi.org/10.1016/j.bbamcr.2015.09.011 (2015).

24   Jo, A. *et al.* Efficient Mitochondrial Genome Editing by CRISPR/Cas9. *BioMed research international* **2015**, 305716, doi:10.1155/2015/305716 (2015).

25   Loutre, R., Heckel, A.-M., Smirnova, A., Entelis, N. & Tarassov, I. Can Mitochondrial DNA be CRISPRized: Pro and Contra. *IUBMB life* **70**, 1233-1239, doi:10.1002/iub.1919 (2018).

26   Bian, W. P. *et al.* Knock-In Strategy for Editing Human and Zebrafish Mitochondrial DNA Using Mito-CRISPR/Cas9 System. *ACS synthetic biology* **8**, 621-632, doi:10.1021/acssynbio.8b00411 (2019).

27   Hussain, S.-R. A., Yalvac, M. E., Khoo, B., Eckardt, S. & McLaughlin, K. J. Adapting CRISPR/Cas9 System for Targeting Mitochondrial Genome. *bioRxiv*, 2020.2002.2011.944819, doi:10.1101/2020.02.11.944819 (2020).

28   Yoo, B.-C., Yadav, N. S., Orozco, E. M., Jr. & Sakai, H. Cas9/gRNA-mediated genome editing of yeast mitochondria and Chlamydomonas chloroplasts. *PeerJ* **8**, e8362, doi:10.7717/peerj.8362 (2020).

29   Gammage, P. A., Moraes, C. T. & Minczuk, M. Mitochondrial Genome Engineering: The Revolution May Not Be CRISPR-Ized. *Trends in genetics : TIG* **34**, 101-110, doi:10.1016/j.tig.2017.11.001 (2018).

30   Moberg, P. *et al.* NMR solution structure of the mitochondrial F1beta presequence from Nicotiana plumbaginifolia. *Journal of molecular biology* **336**, 1129-1140, doi:10.1016/j.jmb.2004.01.006 (2004).

31   Saitoh, T. *et al.* Tom20 recognizes mitochondrial presequences through dynamic equilibrium among multiple bound states. *The EMBO journal* **26**, 4777-4787, doi:10.1038/sj.emboj.7601888 (2007).

32   Yamano, K. *et al.* Tom20 and Tom22 share the common signal recognition pathway in mitochondrial protein import. *The Journal of biological chemistry* **283**, 3799-3807, doi:10.1074/jbc.M708339200 (2008).

33   Tamura, Y. *et al.* Tim23-Tim50 pair coordinates functions of translocators and motor proteins in mitochondrial protein import. *The Journal of cell biology* **184**, 129-141, doi:10.1083/jcb.200808068 (2009).

34   Chacinska, A., Koehler, C. M., Milenkovic, D., Lithgow, T. & Pfanner, N. Importing mitochondrial proteins: machineries and mechanisms. *Cell* **138**, 628-644, doi:10.1016/j.cell.2009.08.005 (2009).

35   Jeandard, D. *et al.* Import of Non-Coding RNAs into Human Mitochondria: A Critical Review and Emerging Approaches. *Cells* **8**, doi:10.3390/cells8030286 (2019).

36   Rubio, M. A. *et al.* Mammalian mitochondria have the innate ability to import tRNAs by a mechanism distinct from protein import. *Proceedings of the National Academy of*

Sciences of the United States of America **105**, 9186-9191, doi:10.1073/pnas.0804283105 (2008).

37   Mercer, T. R. *et al.* The human mitochondrial transcriptome. *Cell* **146**, 645-658, doi:10.1016/j.cell.2011.06.051 (2011).

38   Wang, G. *et al.* PNPASE regulates RNA import into mitochondria. *Cell* **142**, 456-467, doi:10.1016/j.cell.2010.06.035 (2010).

39   Cameron, T. A., Matz, L. M. & De Lay, N. R. Polynucleotide phosphorylase: Not merely an RNase but a pivotal post-transcriptional regulator. *PLoS genetics* **14**, e1007654, doi:10.1371/journal.pgen.1007654 (2018).

40   Mohanty, B. K. & Kushner, S. R. Polynucleotide phosphorylase functions both as a 3' right-arrow 5' exonuclease and a poly(A) polymerase in Escherichia coli. *Proceedings of the National Academy of Sciences of the United States of America* **97**, 11966-11971, doi:10.1073/pnas.220295997 (2000).

41   Yehudai-Resheff, S., Hirsh, M. & Schuster, G. Polynucleotide phosphorylase functions as both an exonuclease and a poly(A) polymerase in spinach chloroplasts. *Molecular and cellular biology* **21**, 5408-5416, doi:10.1128/mcb.21.16.5408-5416.2001 (2001).

42   Fox, T. D. Mitochondrial protein synthesis, import, and assembly. *Genetics* **192**, 1203-1234, doi:10.1534/genetics.112.141267 (2012).

43   Wang, X.-Y. *et al.* Impact of Different Promoters on Episomal Vectors Harbouring Characteristic Motifs of Matrix Attachment Regions. *Scientific Reports* **6**, 26446, doi:10.1038/srep26446 (2016).

44   Wang, G. *et al.* PNPASE Regulates RNA Import into Mitochondria. *Cell* **142**, 456-467, doi:10.1016/j.cell.2010.06.035 (2010).

45   Larsson, C., Grundberg, I., Söderberg, O. & Nilsson, M. In situ detection and genotyping of individual mRNA molecules. *Nature Methods* **7**, 395-397, doi:10.1038/nmeth.1448 (2010).

46   Peeva, V. *et al.* Linear mitochondrial DNA is rapidly degraded by components of the replication machinery. *Nature Communications* **9**, 1727, doi:10.1038/s41467-018-04131-w (2018).

47   Zhao, L. Mitochondrial DNA degradation: A quality control measure for mitochondrial genome maintenance and stress response. *Enzymes* **45**, 311-341, doi:10.1016/bs.enz.2019.08.004 (2019).

48   Su, X. & Dowhan, W. Translational Regulation of Nuclear Gene COX4 Expression by Mitochondrial Content of Phosphatidylglycerol and Cardiolipin in Saccharomyces cerevisiae. *Molecular and cellular biology* **26**, 743, doi:10.1128/MCB.26.3.743-753.2006 (2006).

49   Abu-Elheiga, L. *et al.* The subcellular localization of acetyl-CoA carboxylase 2. *Proceedings of the National Academy of Sciences* **97**, 1444, doi:10.1073/pnas.97.4.1444 (2000).

50   Bravo-Alonso, I. *et al.* Nonketotic hyperglycinemia: Functional assessment of missense variants in GLDC to understand phenotypes of the disease. *Human Mutation* **38**, 678-691, doi:10.1002/humu.23208 (2017).

51   Bogenhagen, D. F., Rousseau, D. & Burke, S. The layered structure of human mitochondrial DNA nucleoids. *The Journal of biological chemistry* **283**, 3665-3675, doi:10.1074/jbc.m708444200 (2008).

52   Prasannan, P., Pike, S., Peng, K., Shane, B. & Appling, D. R. Human mitochondrial C1-tetrahydrofolate synthase: gene structure, tissue distribution of the mRNA, and immunolocalization in Chinese hamster ovary calls. *The Journal of biological chemistry* **278**, 43178-43187, doi:10.1074/jbc.m304319200 (2003).

53   Walkup, A. S. & Appling, D. R. Enzymatic characterization of human mitochondrial C1-tetrahydrofolate synthase. *Archives of Biochemistry and Biophysics* **442**, 196-205, doi:https://doi.org/10.1016/j.abb.2005.08.007 (2005).

Appendix
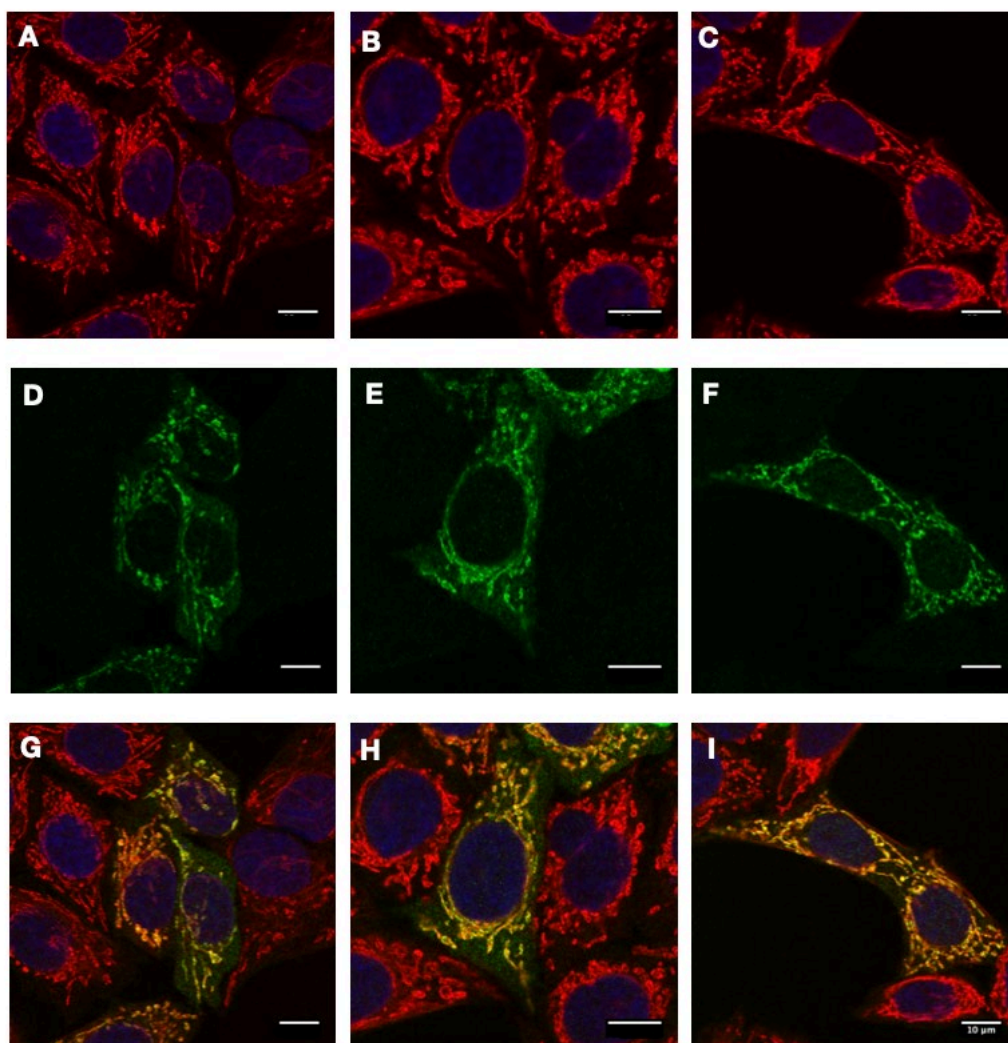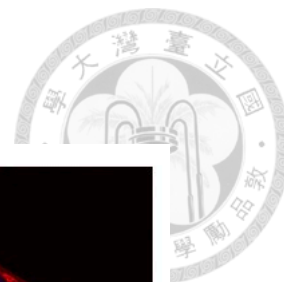
Supplementary figure 1. Immunofluorescence images of mito-Cas9

MTS from mitochondrial monofunctional C1-tetrahydrofolate synthase, 1-38 aa, was found to be the efficient MTS for mitochondrial import of Cas9. (A-C) HeLa cells with nuclei stained by DAPI (blue) and mitochondria stained by MitoTracker Deep Red (red). (D-F) HeLa cells with mito-Cas9 detected by anti-FLAG primary antibody and Alexa Fluor 488-conjugated secondary antibody (green). (G-I) Merged images of A-F showed the co-localization of mitochondria and mito-Cas9 (orange). The experiment was conducted by Michael Feng.
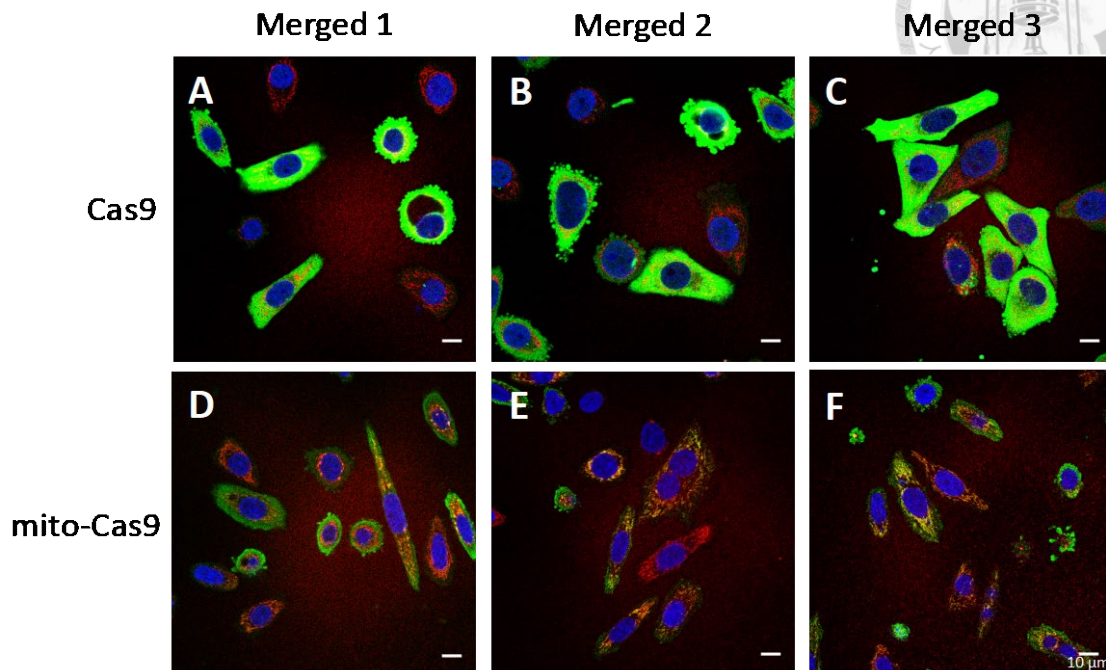
Supplementary figure 2. Mito-Cas9 over-expression results in aberrant morphology

The gene expression of both Cas9 and mito-Cas9 could eventually cause toxic effect to the cells over time that changes the cell morphology. (A-C) HeLa cells with Cas9 over-expression. (D-F) HeLa cells with mito-Cas9 over-expression. Blue signal, nuclei stained by DAPI. Red signal, mitochondria stained by MitoTracker Deep Red. Green signal, Cas9 detected by anti-FLAG primary antibody and Alexa Fluor 546-conjugated secondary antibody. The experiment was conducted by Michael Feng.
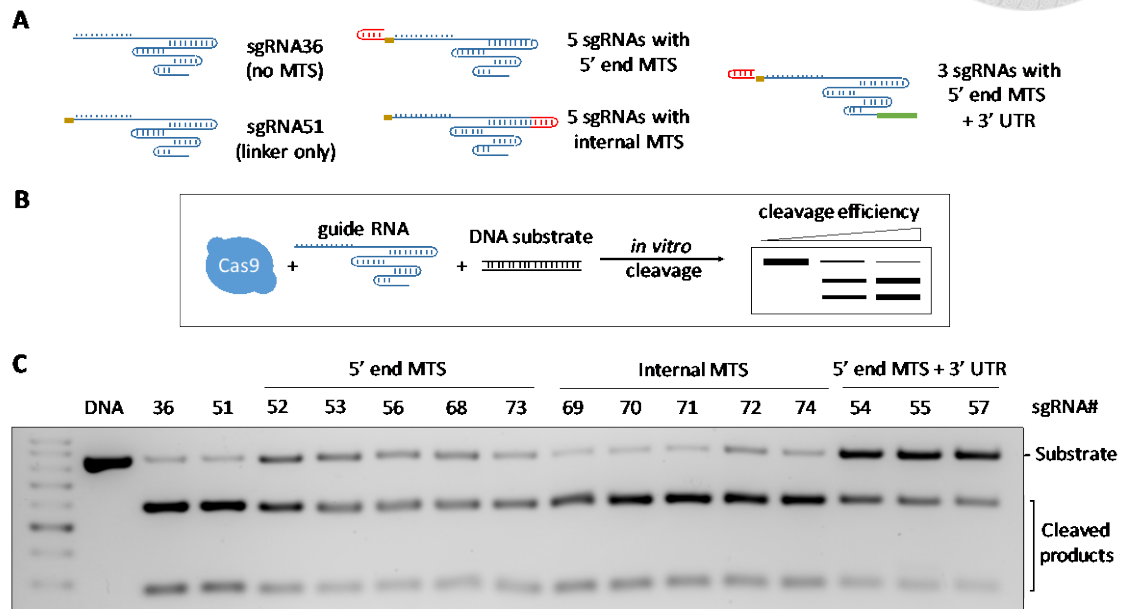
Supplementary figure 3. *In vitro* **cleavage assay of mito-sgRNAs**

The mito-sgRNAs maintained their endonuclease activities after sequence

modifications. (A) Mito-sgRNAs can be classified based on the modified regions of the

sgRNAs to 5' end modification, internal modification, and 5' end modification with 3'

UTR. (B) Schematic flow diagram of *in vitro* cleavage assay. The ND4 DNA substrate

was incubated with Cas9 and mito-sgRNA ribonucleoprotein, and the cleavage

efficiency was determined by the intensity of cleavage products. (C) The *in vitro*

cleavage assay showed the internal modifications could maintain the highest

endonuclease activity comparable to non-modified sgRNA and sgRNA with 10-

nucleotide linker. The experiment was conducted by Michael Feng.
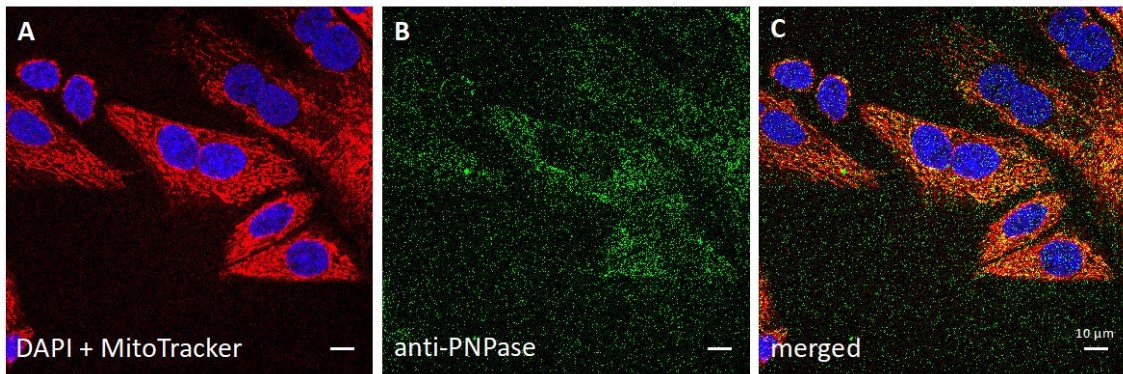
Supplementary figure 4. PNPase exists in HeLa mitochondria

PNPase was found to co-localize with mitochondria within the cells. (A) HeLa cells with nuclei stained by DAPI (blue) and mitochondria stained by MitoTracker Deep Red (red). (B) HeLa cells with PNPase detected by anti-PNPase primary antibody and Alexa Fluor 488-conjugated secondary antibody (green). (C) Merged images of A&B showed the co-localization of mitochondria and PNPase (yellow). The experiment was conducted by Michael Feng.
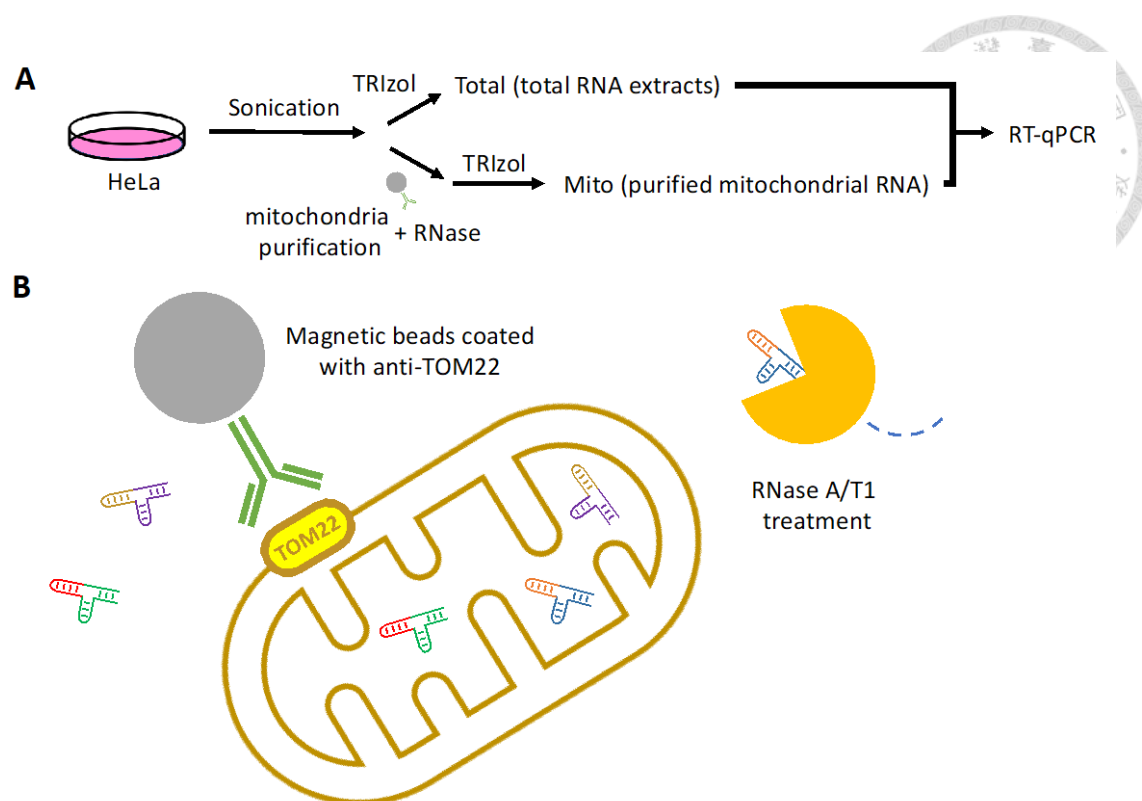
Supplementary figure 5. Schematic flow chart for mitochondrial RNA extraction

(A) To extract the total RNA and mitochondrial RNA, the HeLa cells were lysed by

sonication. A portion of the lysate went through TRIzol-mediated RNA recovery for

total RNA extraction. The rest of the lysate went through mitochondria purification and

RNase A/T1 treatment followed by TRIzol-mediated RNA recovery to extract the

mitochondrial RNA. Then, RT-PCR was performed to analyze the translocation rates of

3 nuclear encoded non-coding RNAs that was known for being imported into the

mitochondria by PNPase. (B) To ensure the mitochondrial RNA purity, the

mitochondria were purified by anti-TOM22-conjugated beads from the cell lysate. The

purified mitochondria were treated with RNase A/T1 to ensure degradation of the non-

mitochondrial RNAs before mitochondrial RNA extraction.

Concept

$$\text{Translocation ratio} = \frac{[\text{target RNA}]_{\text{Mito}}}{[\text{target RNA}]_{\text{Total}}}$$

Formula

$$\Delta\Delta Ct = \Delta Ct_{\text{Mito}}(\text{target-M16S}) - \Delta Ct_{\text{Total}}(\text{target-M16S})$$
$$\text{Ratio} = 2^{-\Delta\Delta Ct}$$

Example

Sample	Target	Cт	ΔCт	ΔΔCт	Ratio
Mito	5.8S	30.0	=30-24.2=5.8	=5.8-(-4.2)	=2^(-10)
Mito	M16S	24.2		=10	=0.1%
Total	5.8S	16.7	=16.7-20.9=-4.2		
Total	M16S	20.9			

Mito = purified mitochondrial RNA   5.8S = 5.8S rRNA (cytosolic)
Total = total RNA extracts   M16S = M16S rRNA (mitochondrial)

Supplementary figure 6. Mitochondrial translocation rate formulation

To calculate the mitochondrial translocation rates of the nuclear encoded non-coding RNAs, the ratio of the RNA amount in mitochondria to the RNA amount in the cell was obtained by the conversion of Ct value from qPCR analysis. The RNA amounts were normalized to the respective M16S level. Then, the mitochondrial amount was compared to the cellular amount by calculating the ΔΔCt value. The translocation rate can be determined by the value of $2^{-\Delta\Delta Ct}$.

RT-qPCR
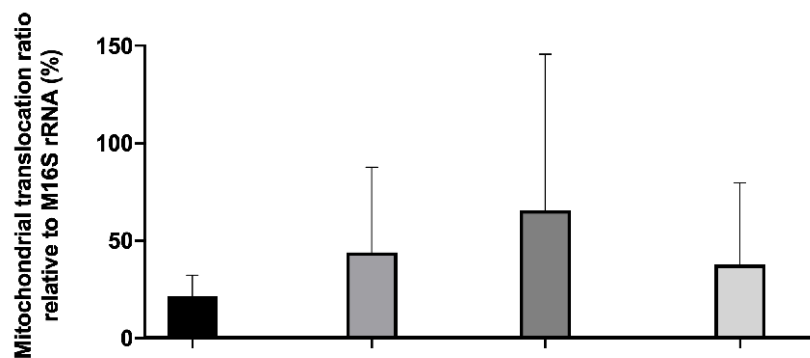
| M16S rRNA	5.8S rRNA	5S rRNA	RNase P RNA	RNase MRP RNA	**Name**
mtDNA	nuclear DNA	nuclear DNA	nuclear DNA	nuclear DNA	**Encoded by**
mitochondria	cytosol	cytosol (mainly) & mitochondria	cytosol (mainly) & mitochondria	cytosol (mainly) & mitochondria	**Localizaion**

Supplementary figure 7. PNPase-mediated nuclear-encoded RNAs exist in HeLa mitochondria

The RT-qPCR analysis of mitochondrial translocation rate demonstrated the existence of PNPase-mediated nuclear-encoded RNAs within the mitochondria. The RNAs, 5S rRNA, RNase P RNA, RNase MRP RNA all showed high translocation rate compared to 5.8S rRNA, a nuclear-encoded cytosolic ribosomal RNA. The experiment was conducted by Michael Feng.
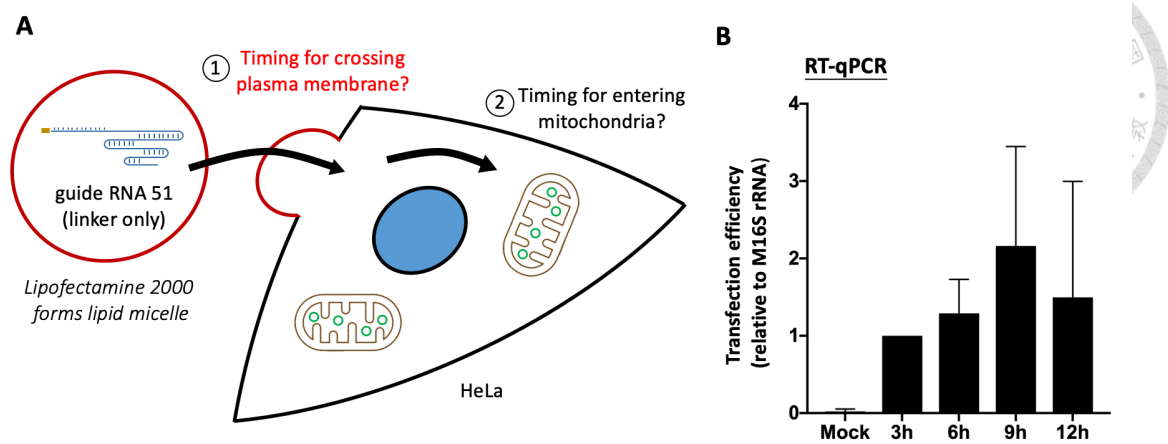
Supplementary figure 8. Schematic flow chart for time-course abundance of mito-sgRNA51 in HeLa cells

(A) Mito-sgRNA51 is used as the representative mito-sgRNA for determination of mito-sgRNA time course transfection efficiency into HeLa cells by Lipofectamine 2000 reagent. (B) After mito-sgRNA51 transfection, the cells were incubated for three to 12 hours and the total RNA was extracted for RT-qPCR analysis. The mito-sgRNA51 abundance relative to M16S was highest at nine hours post-transfection time point. The experiment was conducted by Michael Feng.
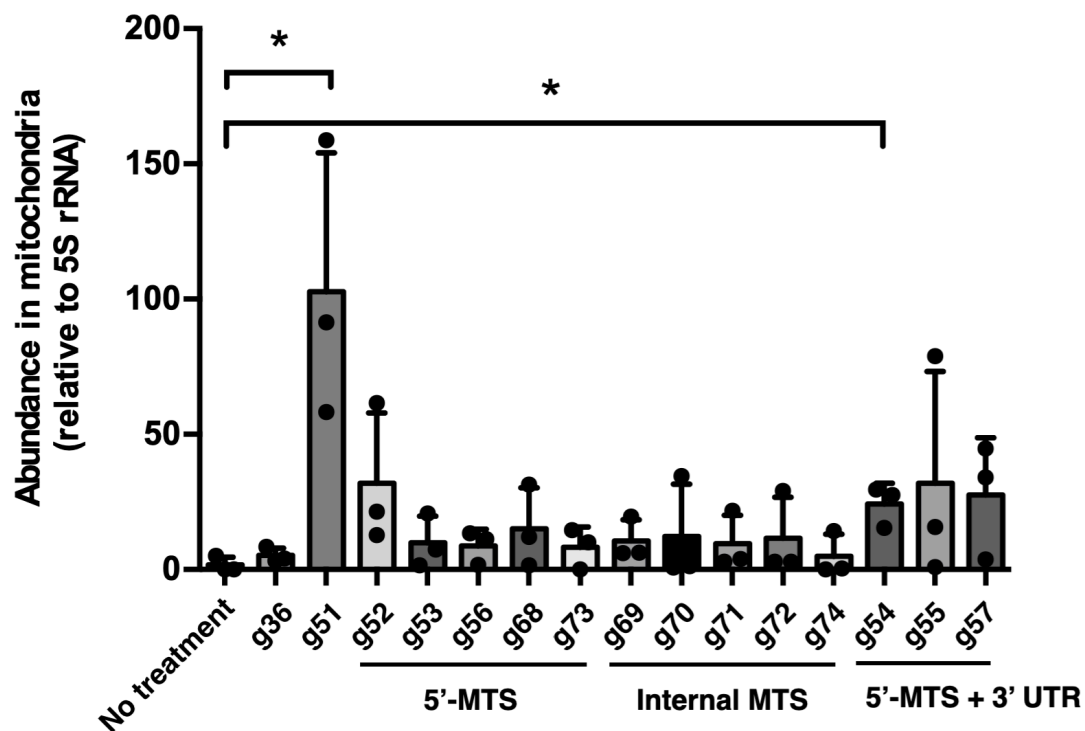
Supplementary figure 9. Mito-sgRNA import efficiency

The RT-qPCR analysis demonstrated the abundance of our mito-sgRNAs relative to 5S rRNA in the mitochondria. Mito-sgRNA51, which is the sgRNA with a 10-nucleotide linker showed the highest abundance in mitochondria, indicating the most efficient mito-sgRNA for mitochondria import (n=3, one-tailed t-test P<0.05). The experiment was conducted by Michael Feng.